SNX-BAR proteins 5 and 6 are required for NCOA7-AS antiviral activity against influenza A virus

Mary Arnaud-Arnould[1*], Antoine Rebendenne[1,4,5*], Marine Tauziet[1], Serge Urbach[2], Khadija El Koulali[3], Emiliano Ricci[4], Mélanie Wencker[4,5], Olivier Moncorgé[1], Mickaël Blaise[1,@] and Caroline Goujon[1,@]

1 IRIM, CNRS, Montpellier University, Montpellier, France.

2 IGF, Montpellier University, CNRS, INSERM, Montpellier, France.

3 BCM, Montpellier University, CNRS, INSERM, Montpellier, France.

4 LBMC, INSERM, CNRS, ENS-Lyon, Lyon University, Lyon, France.

5 CIRI, INSERM, CNRS, ENS-Lyon, Lyon University, Lyon, France.

* Contributed equally to the work

@ correspondence to: mickael.blaise@irim.cnrs.fr; caroline.goujon@irim.cnrs.fr

Abstract

Interferon-induced antiviral proteins act on the first line of defence against viruses, including influenza A virus (IAV). Among those, the short isoform of Nuclear Receptor Coactivator 7 (NCOA7-AS) has been shown to inhibit IAV entry and more especially the fusion between endosomal and viral membranes. Ectopic expression of NCOA7-AS leads to the increased acidification of the endolysosomal pathway, putatively through NCOA7-AS interaction with the vacuolar ATPase (V-ATPase). However, the precise mechanism of action of NCOA7-AS is not fully understood. Here, we identified the cellular partners of NCOA7-AS by mass spectrometry, including the V-ATPase subunits known to interact with NCOA7-AS. Mutation of NCOA7-AS glycine 91 abolished V-ATPase binding and antiviral activity against IAV, confirming the role of the V-ATPase in the antiviral phenotype. Moreover, sorting nexin (SNX) 1/2/5/6 were identified as novel partners of NCOA7-AS. These proteins are involved in retrograde transport of cellular cargoes from endosomes to the trans-Golgi network. We revealed that SNX5/6 were essential for NCOA7-AS antiviral activity against IAV and interacted directly with NCOA7-AS. Interestingly, crystal structures of NCOA7-AS/SNX5 complexes showed that the SNX5-interaction motif in NCOA7-AS was similar to those found in known cargoes of SNX5/6. In addition, we could pinpoint several critical residues that were important for binding and antiviral activity. Collectively, our study identifies novel essential partners for NCOA7-AS antiviral activity and the structural basis for their interaction.

Introduction

Seasonal influenza A viruses (IAV) pose a major threat to global health, putting significant pressure on healthcare systems and causing significant morbidity and mortality each year, according to the World Health Organization. IAV are respiratory viruses, belonging to the *Orthomyxoviridae* family, that cause mild to moderate upper respiratory tracts illnesses. Successful infection of host cells by IAV depends on a complex, multi-step entry process. The hemagglutinin (HA) protein of human-adapted strains of IAV interacts preferentially with glycoconjugates bearing terminal α-2,6-linked sialic acids (reviewed in (Dou et al., 2018)). Then, IAV particle is internalized through endocytosis (Matlin et al., 1981). This early event requires numerous host factors that belong to the endocytic pathway and to the vacuolar ATPase (V-ATPase) complex, responsible for the gradual lumen acidification of endosomes. The V-ATPase is a multi-subunit complex, composed of two distinct domains: the membrane-associated V0 domain, which is responsible for proton translocation to the lumen of the vesicle, and the cytoplasmic V1 domain, which provides energy by ATP hydrolysis (reviewed in (Cotter et al., 2015)). Endosomal acidification by the V-ATPase is critical for HA acidification, fusion peptide exposure and subsequent HA-mediated fusion between viral and endosomal membranes. Furthermore, luminal acidification activates the viral M2 ion channel, leading to acidification and increase proton concentration inside the viral particle (Pinto et al., 1992; Wharton et al., 1994; Pinto and Lamb, 2006; Stauffer et al., 2014). This induces conformational changes in the matrix protein M1, disrupting the viral capsid and the interaction between M1 and the viral ribonucleoproteins complexes (vRNPs), leading to the subsequent release of vRNPs in the cytoplasm (Zhirnov, 1990; Helenius, 1992).

IAV entry is a critical step targeted by many potent antiviral proteins, including some coded by interferon-stimulated genes (ISGs) that are part of the interferon (IFN) system. The IFNs act as one of the first lines of defence against viral infections (reviewed in (Villalón-Letelier et al., 2017; McKellar et al., 2021)). Notably, the interferon-inducible, short isoform of Nuclear Receptor Coactivator 7 (NCOA7), NCOA7-Alternative-Start (NCOA7-AS, also called NCOA7-B) has been shown to inhibit IAV virus entry (Doyle et al., 2018) as well as endosome-mediated coronavirus entry (Khan et al., 2021; Wickenhagen et al., 2021). NCOA7-AS belongs to the Tre2/Bub2/Cdc16 (TBC), lysin motif (LysM), domain catalytic (TLDc)-containing family of proteins. Despite their name, no enzymatic activity has ever been reported for TLDc-bearing proteins (Blaise et al., 2012), but they have been shown to protect cells from oxidative stress, by an unknown mechanism (Finelli and Oliver, 2017). Interestingly, the TLDc proteins are known interactors of the V-ATPase (Merkulova et al., 2015; Eaton et al., 2021). Ectopic expression of NCOA7-AS increases acidification of the endolysosomal pathway, supposedly through NCOA7-

AS interaction with the V-ATPase (Doyle et al., 2018). NCOA7-AS ectopic expression is also associated with a decrease in IAV/endolysosomal membrane fusion. However, the precise molecular mechanism of action of NCOA7-AS is yet to be unraveled.

Here, we used mass spectrometry to identify the cellular partners of NCOA7-AS, and confirmed its interaction with V-ATPase subunits. A single amino acid substitution on NCOA7-AS glycine 91 disrupted its association with the V-ATPase and prevented antiviral activity against IAV, highlighting the importance of this interaction in mediating the antiviral effect. Additionally, sorting nexins SNX1, SNX2, SNX5, and SNX6 were identified as novel binding partners of NCOA7-AS. These proteins are known to play roles in retrograde transport of cellular cargoes to the trans-Golgi network (Burd and Cullen, 2014). We demonstrated that SNX5 and SNX6 bind directly to NCOA7-AS' amino-terminal domain and were required for IAV inhibition. Moreover, crystal structures of NCOA7-AS in complex with SNX5 revealed that the SNX5-binding motif in NCOA7-AS resembles those found in established SNX5/6 cargoes (Simonetti et al., 2019). Collectively, these findings suggest that NCOA7-AS uses SNX proteins to suppress IAV replication.

Results

The interaction between NCOA7-AS and V1 subunits of the V-ATPase is required for antiviral activity

TLDc proteins are known interactors of the V-ATPase (Merkulova et al., 2015; Eaton et al., 2021). Notably, the long isoform of NCOA7 (herein called NCOA7-FL) and NCOA7-AS have been shown to interact with V1 subunits of the V-ATPase (ATP6V1B1/2 and also A, C and G) and to promote endolysosomal acidification (Merkulova et al., 2015; Doyle et al., 2018; Castroflorio et al., 2021). As shown previously, several amino acids in TLDc proteins are well conserved across different species and are important to bind the V-ATPase (Eaton et al., 2021). Notably, mutations of glycine 815, glycine 845 and glycine 896 in mouse NCOA7-FL abolished interaction with the V-ATPase (Eaton et al., 2021). Among these 3 residues, only glycine 815 is exposed on the surface of the TLDc, therefore the focus was made on the equivalent glycine in NCOA7-AS (glycine 91). As shown by docking of NCOA7-AS AlphaFold model on the Cryo-EM structure of human V-ATPase bound to another TLDc domain containing protein, mEAK7 (Wang et al., 2022), this glycine 91 is present on a short loop in close proximity to the V-ATPase subunit B (Figure 1A). In order to study its importance, glycine 91 was mutated to an alanine (G91A). Lung-derived A549 cells were transduced to stably express a negative control (Firefly), wild-type NCOA7-AS (NCOA7-AS-WT) or NCOA7-AS-G91A mutant. Co-immunoprecipitation experiments confirmed that NCOA7-AS interacted with V1 subunits of the V-ATPase, namely ATP6V1A, ATP6V1B2 and ATP6V1E1, while NCOA7-AS-G91A mutant was unable to interact with these subunits (Figure 1B).

To determine whether interactions of NCOA7-AS with the V-ATPase were indeed required for antiviral activity and overacidification of the endolysosomal compartment, NCOA7-AS-G91A antiviral activity was tested against Nanoluciferase-encoding influenza reporter viruses A/Victoria/3/75 (H3N2) and A/WSN/1933 (H1N1) in single-cycle experiments. Ectopic expression of NCOA7-AS-WT led to a strong inhibition of A/Victoria/3/75 and A/WSN/1933 infection (Figure 1C-D), while NCOA7-AS-G91A mutant showed almost no antiviral activity. Furthermore, the endosomal/lysosomal compartment size and relative acidification levels were assessed using LysoTracker and LysoSensor reagents, respectively. This confirmed that NCOA7-AS-WT induced a significant expansion of the acidic compartments (Figure 1E) and a decrease in endosomal/lysosomal pH (Figure 1F). In contrast, NCOA7-AS-G91A mutant had no impact as the values were similar to the negative control condition, strongly arguing that the interaction of NCOA7-AS with the V-ATPase is required for antiviral activity against IAV and overacidification of the endolysosomal compartment.

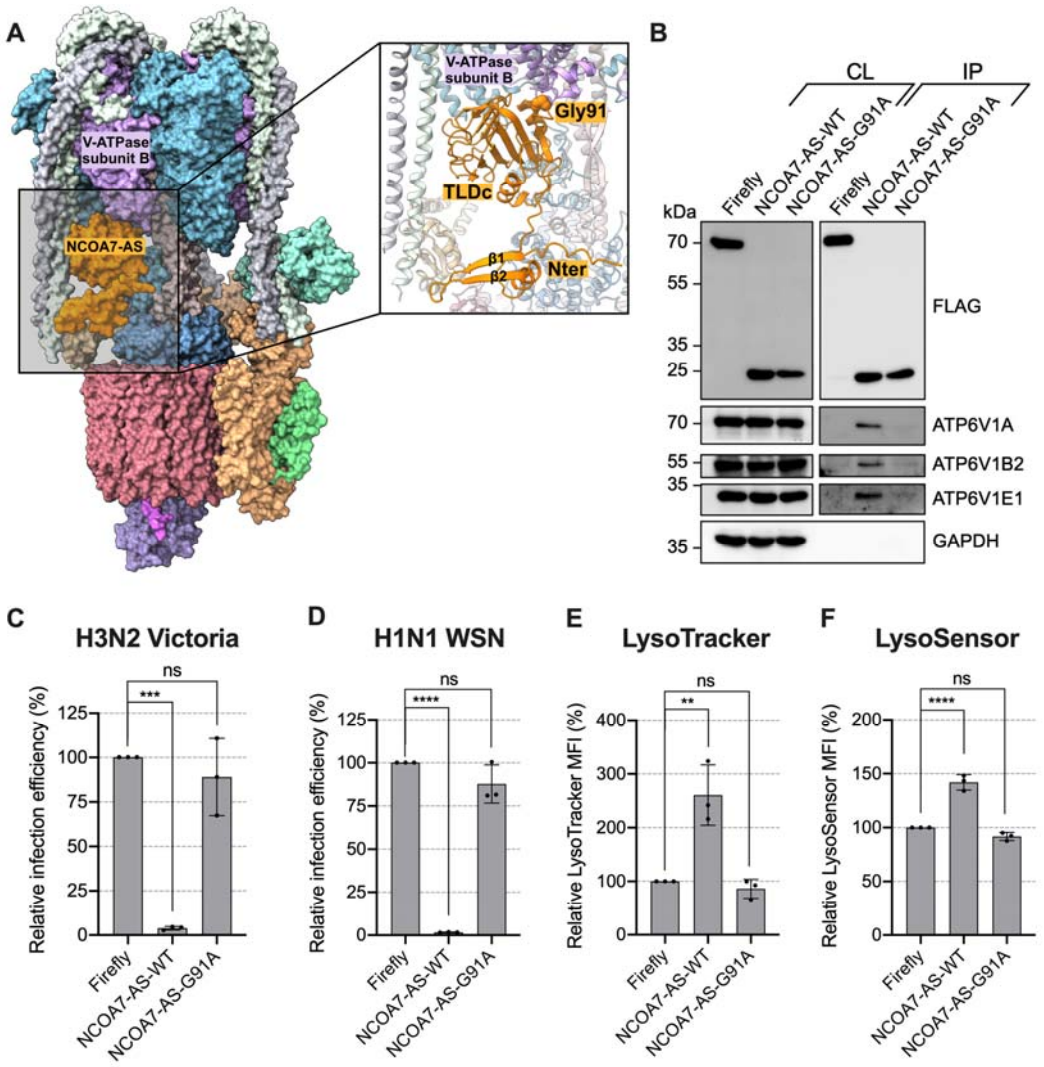

Figure 1. NCOA7-AS G91 is essential for V-ATPase binding, antiviral activity against IAV, and endolysosomal compartment overacidification. A. Docking of NCOA7-AS AlphaFold model on the Cryo-EM structure of human V-ATPase bound to mEAK7, a TLDc domain containing protein (PDB:7unf). The NCOA7-AS model (in orange) was superposed onto the TLDc domain of mEAK7 using ChimeraX. The zoom panel indicates that the loop harboring NCOA7-AS G91, shown as spheres, is in close proximity to the V-ATPase subunit **B.** A549 cells were transduced with lentiviral vectors expressing FLAG-tagged Firefly (a negative control), NCOA7-AS-WT or NCOA7-AS-G91A. Cells were lysed and the FLAG-tagged proteins were immunoprecipitated and subsequently analyzed by immunoblotting using anti-GAPDH (loading control), anti-FLAG, anti-ATP6V1A, anti-ATP6V1B2 and anti-ATP6V1E1 antibodies. **C-D.** Cells stably expressing FLAG-tagged Firefly (Control), NCOA7-AS-WT or NCOA7-AS-G91A were infected with IAV (A/Victoria/3/75) encoding a Nanoluciferase reporter gene at an MOI of 0.5 (**C**) or with IAV (A/WSN/1933) encoding a Nanoluciferase reporter gene at an MOI of 0.25 (**D**). The relative infection efficiency was measured by monitoring Nanoluciferase activity 8h post-infection. **E-F.** Cells stably expressing FLAG-tagged Firefly (Control), NCOA7-AS-WT or NCOA7-AS-G91A were treated with 0.1 µM LysoTracker Green DND-26 (**E**) or with 0.1 µM LysoSensor Green DND-189 (**F**) for 1h at 37°C and subsequently analyzed by flow cytometry. (**C-F**) Results were normalized to 100% for the control condition (Firefly), and the mean and SD of three independent experiments are shown.

SNX5/6 are cellular partners of NCOA7-AS and are important for its antiviral activity

To identify novel binding partners of NCOA7-AS, 3xFLAG-tagged NCOA7-AS was stably expressed in glioblastoma-derived U87-MG cells, immunoprecipitated and the immunoprecipitates analyzed by mass spectrometry (Supplementary Table 1). The interaction between NCOA7-AS and several V1 subunits of the V-ATPase, namely ATP6V1A, ATP6V1B2, ATP6V1C1, ATP6V1D, ATP6V1E1, and ATP6V1G1, was confirmed (Figure 2A, Supplementary Table 1). The NCOA7-AS interactome additionally contained four members of the sorting nexins (SNX) family, SNX1, SNX2, SNX5 and SNX6, which were particularly enriched (Figure 2A). SNX proteins are important for retrograde transport of proteins between endosomes and the trans-Golgi network (Burd and Cullen, 2014).

SNX proteins notably contain a Phox homology (PX) domain, and some of them are known to interact with phosphoinositides. Hence PX-SNX1 and PX-SNX2 interact with phosphatidylinositol-3-phosphate at the endosomal membrane (Cheever et al., 2001; Yu and Lemmon, 2001; Burda et al., 2002; Gillooly et al., 2003) but not PX-SNX5 and PX-SNX6 (Chandra et al., 2019). SNX1/2/5/6 belong to the SNX-BAR subfamily, and possess a Bin-Amphiphysin-Rvs (BAR) domain. The BAR domain is important for dimerization and to detect and/or induce membrane curvature (Carlton et al., 2004; Frost et al., 2009; Weering et al., 2010). A heterodimer of SNX-BAR proteins, consisting of SNX1 or SNX2 associated with either SNX5 or SNX6, forms the Retromer complex in association with a vacuolar protein sorting (VPS) trimer. The Retromer complex mediates cargo trafficking from the endosome to the trans-Golgi network (Wassmer et al., 2006). However, recent studies have shown that some cargoes could be transported by a SNX1/2-SNX5/6-dependent pathway that was Retromer-independent (Kvainickas et al., 2017; Simonetti et al., 2017; Yong et al., 2020). Interestingly, an additional, non-canonical role has also been reported for SNX5. Indeed, SNX5 has been shown to inhibit several viruses, including IAV, by inducing autophagy at virus-containing endosomes independently of SNX1, SNX2 or the Retromer complex (Dong et al., 2021).

The interaction between NCOA7-AS and these four SNX-BAR proteins was confirmed by co-immunoprecipitation experiments followed by western blot analysis. Endogenous SNX1, SNX2, SNX5 and SNX6 were co-immunoprecipitated with stably expressed FLAG-tagged NCOA7-AS-WT but not with the FLAG-tagged E2-Crimson negative control in U87-MG cells (Figure 2B).

To assess the role of SNX1, SNX2, SNX5 and SNX6 in NCOA7-AS antiviral activity against IAV and the overacidification of the endolysosomal compartment, control (E2-crimson)- or NCOA7-AS-expressing A549 cells were transfected with non-targeting siRNA (siCTRL) or siRNAs targeting SNX1, SNX2, SNX5 and SNX6. As SNX1/2 on the one hand and SNX5/6 on the other hand were shown to play

redundant roles (Simonetti et al., 2017), SNX1/2 and SNX5/6 double knockdowns were used to circumvent the redundancy. Strikingly, the double depletion of SNX1/SNX2 impaired IAV infection efficiency in the absence of NCOA7-AS but not in its presence, and markedly reduced the ability of NCOA7-AS to modulate endolysosomal pH (Figure 2C-D). In sharp contrast, SNX5/SNX6 depletion had no effect on IAV infection without NCOA7-AS, but significantly rescued infection when NCOA7-AS was expressed (Figure 2C). Furthermore, SNX5/SNX6 depletion tended to attenuate the NCOA7-AS–mediated acidification of endolysosomal compartments, although this effect did not reach statistical significance (Figure 2D). Western blot analyses confirmed the successful reduction of the levels of targeted proteins (Figure 2E). Of note, each double knockdown affected the stability of the overall heterodimer, as shown previously (Simonetti et al., 2017). Whereas relatively similar depleted levels of all four SNXs were detected in each double knockdown condition, only the double knockdown of SNX5/6 could partially rescue viral infection in the presence of NCOA7-AS. This strongly suggested that only a pool of SNX5/6, which could presumably act independently of SNX1/2, was important for NCOA7-AS antiviral activity.

Taken together, these data showed that SNX1 and 2 potentially played a major role in NCOA7-AS-mediated acidification of endolysosomes, whereas only SNX5 and 6 were important for its antiviral activity against IAV.

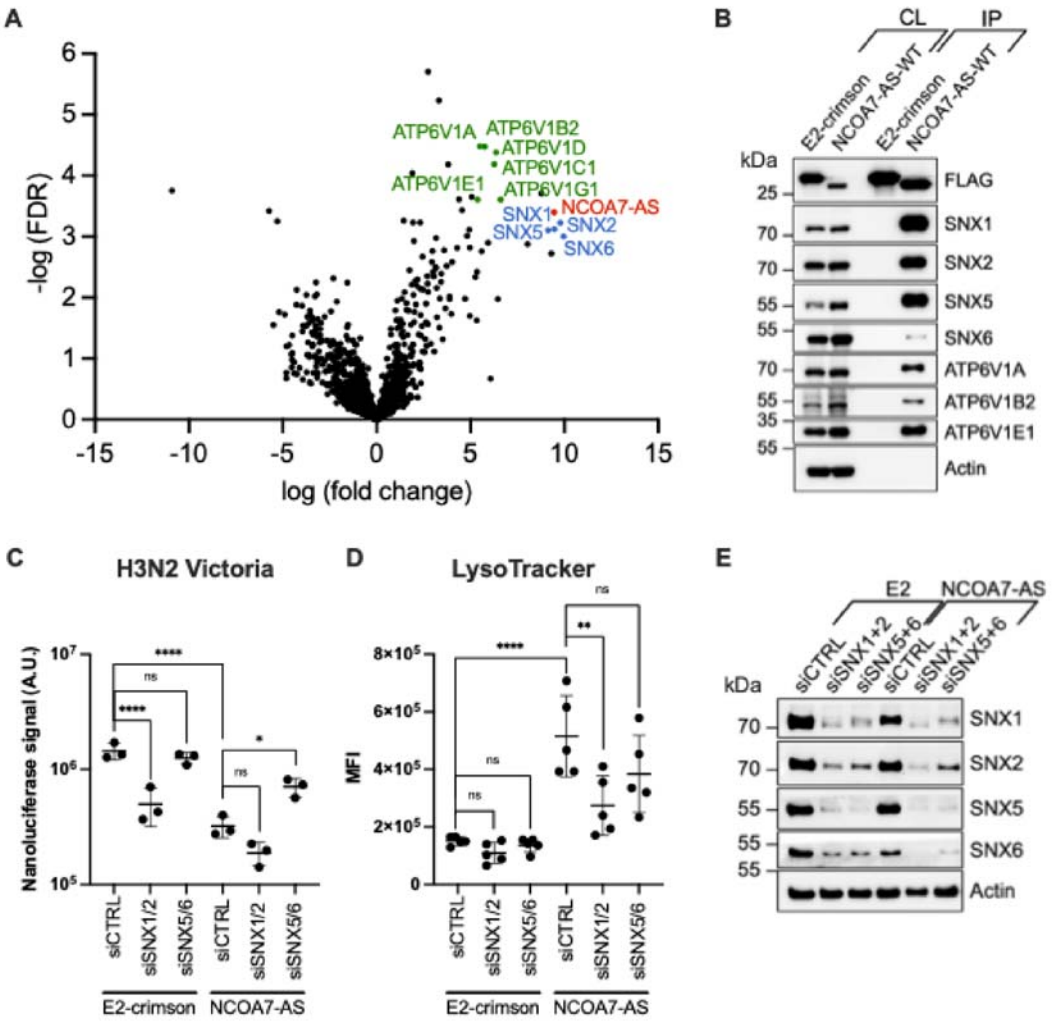

Figure 2. SNX1, SNX2, SNX5 and SNX6 are novel interacting partners of NCOA7-AS that are important for its antiviral activity against IAV. A. Volcano Plot of differentially abundant proteins between NCOA7-AS and control immunoprecipitation, presenting the fold change (in log2) and significance (-Log 10 p value) obtained from a t-test based on intensity values from three independent experiments. **B.** U87-MG cells were transduced with lentiviral vectors expressing FLAG-tagged-NCOA7-AS or -E2-Crimson (a negative control). Cells were lysed and the FLAG-tagged proteins were immunoprecipitated and subsequently analyzed by immunoblotting using anti-actin (loading control), anti-FLAG, anti-SNX1, anti-SNX2, anti-SNX5, anti-SNX6, anti-ATP6V1A, anti-ATP6V1B2 and anti-ATP6V1E1 antibodies, as indicated. **C-D.** A549 cells stably expressing FLAG-tagged-E2-Crimson or -NCOA7-AS were transfected with non-targeting siRNA (siCTRL) or with siRNAs targeting either SNX1 and SNX2, or SNX5 and SNX6. 72h post-transfection, cells were either infected with IAV (A/Victoria/3/75) encoding a Nanoluciferase reporter gene at an MOI of 0.25 and the relative infection efficiency was measured by monitoring Nanoluciferase activity 8h later (**C**) or treated with 0.1 µM LysoTracker Green DND-26 for 1h at 37°C and the mean fluorescent intensity was subsequently analyzed by flow cytometry (**D**). **E.** Representative western blot for **C**-**D**. (**C-D**) The mean and SD of three (**C**) and five (**D**) independent experiments are shown, respectively.

The N-terminal domain of NCOA7-AS directly interacts with the Phox domain of SNX5 and SNX6

SNX5 and SNX6 interact with more than 60 cargoes, including cation-independent mannose-6-phosphate receptor (CI-MPR) (Simonetti et al., 2017, 2019) or *Chlamydia trachomatis* IncE (Mirrashidi et al., 2015; Elwell et al., 2017; Paul et al., 2017; Sun et al., 2017). These interactions are mediated by the PX domain of SNX5 or SNX6 (PX-SNX5 and PX-SNX6). Analysis of the sequence requirement to bind SNX5 or SNX6 revealed that cargoes have a conserved secondary structure, consisting of two antiparallel β-strands with one β-strand containing a ΦxΩxΦ motif, where Φ is a hydrophobic residue and Ω, an aromatic residue (Simonetti et al., 2019).

NCOA7-AS contains two main structural domains: the N-terminal domain (NTD) of 53 amino acids and the TLDc domain, the latter being involved in the interaction with the V-ATPase (Eaton et al., 2021). The structure of the human NCOA7-AS TLDc domain has been recently determined (Arnaud-Arnould et al., 2021), but that of NCOA7-AS-NTD is yet unknown. AlphaFold prediction suggested however that NCOA7-AS-NTD could be organized as two antiparallel β-strands and a small α-helix (Supplementary Figure 1A). Furthermore, the first predicted β-strand contains a ΦxΩxΦ motif (Supplementary Figure 1B), suggesting that NCOA7-AS could directly interact with SNX5 or SNX6.

To test this hypothesis and to map the regions of NCOA7-AS important for SNX binding, different proteins of interest were individually produced in *E. coli* as fusions with Glutathione S-Transferase (GST) or Maltose Binding Protein (MBP) and purified, in order to perform *in vitro* GST pull-down assays. GST-tagged-NCOA7-AS (NCOA7-AS-WT-GST), -NCOA7-AS N-terminal domain (NTD, amino acids 1-53; NCOA7-AS-NTD-GST), -NCOA7-AS TLDc domain (amino acids 54-219) and MBP-tagged-PX-SNX1, -PX-SNX5, -PX-SNX6 were used. The GST pull-downs showed that NCOA7-AS interacted with the PX domains of SNX5 and SNX6 but not with the PX domain of SNX1 (Figure 3A). As previously described by other groups, the PX domains of SNX5 and SNX6 contain a unique 38 amino acid insertion, which folds in a helix-turn-helix extension, that is absent in the PX domains of SNX1 and SNX2 (Simonetti et al., 2019). This insertion has already been shown to be important for the interaction with several cargoes, such as CI-MPR (Simonetti et al., 2019) and IncE (Mirrashidi et al., 2015; Elwell et al., 2017; Paul et al., 2017; Sun et al., 2017).

Furthermore, the ability of NCOA7-AS to bind to the PX domain of SNX5 and SNX6 was mediated by the NTD and not by the TLDc, as shown by the fact that, contrary to NCOA7-AS-NTD-GST, NCOA7-AS-TLDc-GST was not able to bind PX-SNX5 and PX-SNX6 (Figure 3A). Altogether, these results showed that NCOA7-AS directly interacted with SNX5 and SNX6 PX domains via its N-terminal domain.

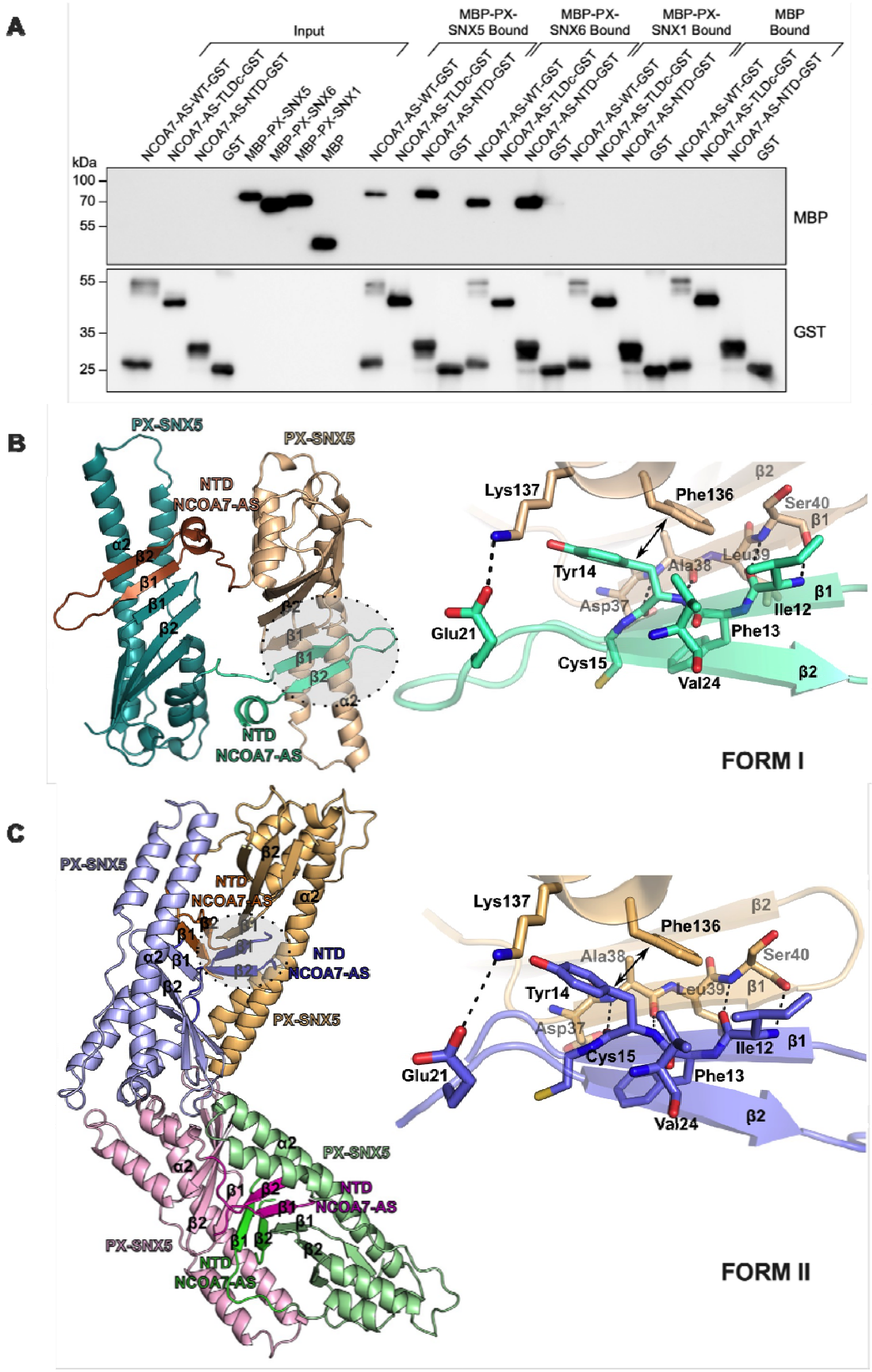

Figure 3. The N-terminal domain of NCOA7-AS interacts directly with the PX domain of SNX5 and SNX6. A. Recombinant MBP-tagged PX-SNX5, PX-SNX6 and PX-SNX1 or MBP alone, and GST-tagged NCOA7-AS-WT, NCOA7-AS-NTD or NCOA7-AS-TLDc or GST alone,

were produced in *Escherichia coli* and purified. GST pull-down assays were performed using these recombinant proteins and analyzed by western blot. **B-C.** Crystal structure of PX-SNX5-NCOA7-AS-NTD chimera. Two crystal forms were solved. In the form I (**B**), the asymmetric unit contains one monomer, the dimer interaction described in here is therefore formed with the symmetric molecule. The second crystal form (**C**) contains four molecules per asymmetric unit and therefore contains two dimers. The overall structures are shown in cartoon representations in **B** and **C**, for all the structures, the NCOA7-AS-NTD is a darker color as compared to the PX-SNX5 domain fused to it. The right panel shows a magnified view of the region, rotated 180° relative to the highlighted zone in grey. The H-bonds interaction between the strands β1 of NCOA7-AS and β1 of the PX domain are shown in black dashed lines. The salt-bridge between Glu21 and Lys137 is also represented by a dashed line. The main interaction between the side chain of Tyr14 from NCOA7-AS and Phe136 of the PX domain is illustrated by the double headed arrows. Val24 also contributes to interact with Phe136 but the interaction is not shown.

In order to better understand the molecular basis of this interaction, we employed a strategy previously described by another team to determine the structure of the two interacting partners (Paul et al., 2017). This strategy consists in designing a chimeric fusion protein with the two binding partners. Such a strategy was successfully used by Prof. Cullen's team to obtain the crystal structure of PX-SNX5 in complex with a peptide from CI-MPR (Simonetti et al., 2019). Therefore, a chimeric protein composed of PX-SNX5 (amino-acids 25-172) and NCOA7-AS N-terminal sequence (amino-acids 4-36) was produced. After recombinant expression in *E. coli* and purification (Supplementary Figure 2A), the chimeric protein was crystallized into two different forms (named forms I and II). The structures of the two distinct crystals were elucidated at high resolution via X-ray crystallography (Figure 3B-C and Supplementary table 2).

PX-SNX5 domain is typically composed of three β-strands (β1, β2 and β3) and three α-helices (α1, α2 and α3) (see PDB: 5wy2). The N-terminus of NCOA7-AS forms a β-hairpin structure consisting of β1 (residues Gln11-Cys15) and β2 strands (residues Phe23-Ile27) and a short α-helix (residues Val29-Arg35). The β-hairpin structure of NCOA7-AS-NTD interacts with PX-SNX5 by forming an anti-parallel β-sheet. The β1 strand of NCOA7-AS strongly interacts by H-bonds with the β-sheet through β1 of the PX-SNX5 domain, and with its complementary groove at the base of the extended α-helical insertion (α2) of the PX-SNX5 domain. The N-terminal β1 strand of NCOA7-AS forms the primary interface with SNX5, by hydrogen bonds involving the main chain with the β1 strand of the PX-SNX5 domain. The two anti-parallel β-strands of NCOA7-AS are connected by a short loop (Ala16-Pro22) that could not be rebuilt in the crystal form II, however, this loop is not making any direct contact with the SNX5 protein in the other form (form I). The NCOA7-AS β1 strand forms an interface of interaction with the extended α-helical region (α2) of the PX-SNX5 domain. This interaction is mediated by several van der Waals interactions but the strongest interaction is driven by the side chain of Tyr14 from β1 strand of NCOA7-AS, through a hydrophobic interaction with the side chain of Phe136 of SNX5. To a lesser extent, Val24 side chain of NCOA7-AS interacts as well with Phe136 of SNX5. A salt-bridge interaction is also established between PX domain Lys137 and NCOA7-AS Glu21. Of note, although the two crystals forms are packing

differently and notably with a different conformation of the NCOA7-AS hairpin in both structures, the β strands interaction and the main interaction between NCOAS-AS Tyr14 and SNX Phe136 are conserved in both structures. This is strongly supportive of a specific interaction not driven by the chimera or the crystal packing. Furthermore, PX-SNX5's mode of interaction with NCOA7-AS was also compared with the previously solved structures of PX-SNX5 bound to other proteins, namely Sema4C (PDB 6n5z; (Simonetti et al., 2019), CI-MPR (PDB 6n5y; (Simonetti et al., 2019) and IncE (PDB 5wy2; (Sun et al., 2017) (Supplementary Figure 2B). This analysis demonstrated that NCOA7-AS interacted in a similar manner as the other interactors of SNX5, by forming an anti-parallel β-sheet and through a hydrophobic interaction between the Phe136 of PX and either a Tyr or a Phe for the different binding partners. Of note, PX-SNX6 is thought to harbor the same binding specificity to cargoes through its Phe137.

To confirm the importance of these residues for the specific interaction seen in the two crystal structures, Phe136 was mutated into Ala (F136A) on MBP-PX-SNX5. *In vitro* GST pull-down assays with NCOA7-AS-WT-GST demonstrated that PX-SNX5 Phe136 was important for NCOA7-AS binding to SNX5 (Figure 4A). In order to gain more insights into this interaction, the dissociation constant (Kd) between PX-SNX5 domain and the N-terminus of NCOA7-AS was measured by microfluidic diffusional sizing (MDS) (Figure 4B). To do so, the hydrodynamic radius (Rh) of a fluorescently labelled NCOA7-AS peptide corresponding to its NTD was measured in solution as well as its Rh in presence of increased concentrations of MBP-PX-SNX5 domain. In parallel, the same experiment was performed with MBP-PX-SNX5-F136A. In absence of ligand, the NCOA7-AS peptide possesses an Rh of about 1.6 nm, while it reaches 3.1 and 2.7 nm at the highest concentration (250 µM) of WT and mutant PX-SNX5, respectively. The titration curve strongly attests that the single point mutation F136A significantly increases the dissociation constant between PX-SNX5 and NCOA7-AS N-terminal domain (Kd=1.6 µM for the PX-SNX5-WT versus 12.4 µM for the F136A mutant). The analysis of the impact of the reciprocal mutation of Tyr14 to Ala on NCOA7-AS (NCOA7-AS-Y14A) confirmed the importance of this residue for the *in vitro* binding to PX-SNX5 (Figure 4C). Of note, NCOA7-AS Val24 mutation to Ala was also tested. *In vitro* GST pull-down assays showed that the interaction between this mutant and PX-SNX5 was slightly decreased but not abolished (data not shown), contrary to what was observed with the Y14A mutant (Figure 4C).

Moreover, Tyr14 was mutated to a minimal conservative Phe substitution, which maintained the aromatic cycle in the lateral chain. Y14F mutation in NCOA7-AS did not affect its ability to bind to PX-SNX5 and SNX6 (Figure 4C), highlighting the fact that the hydrophobic interaction mediated by Tyr14 and Phe136 drives the interaction between NCOA7-AS and SNX5 or SNX6.

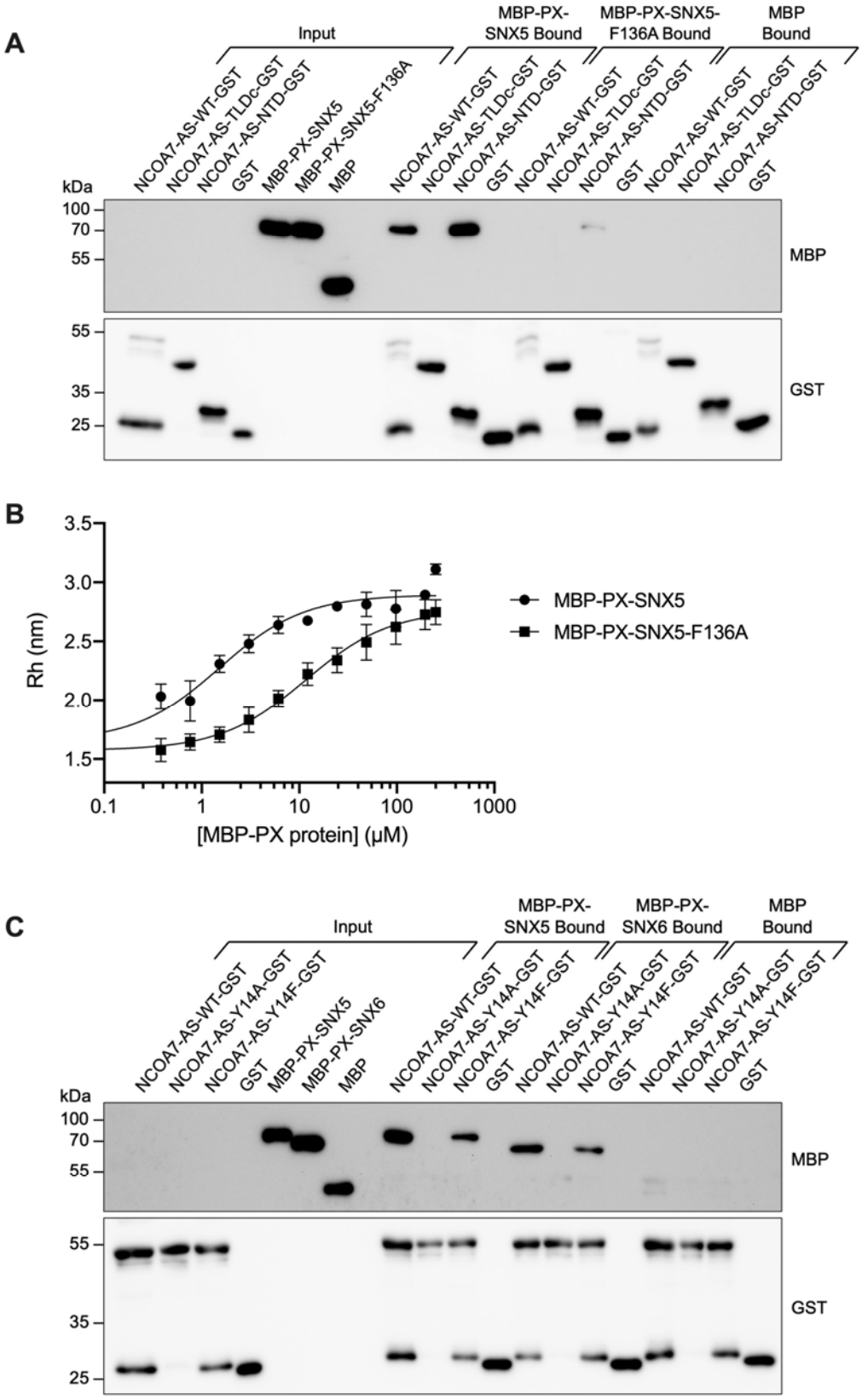

Figure 4. NCOA7-AS-Y14 and SNX5-F136 are important for NCOA7-AS/SNX5 and NCOA7-AS/SNX6 interaction. A. Recombinant MBP-tagged PX-SNX5, PX-SNX5-F136A or MBP alone and GST-tagged NCOA7-AS-WT, NCOA7-AS-NTD, NCOA7-AS-TLDc or GST alone

were produced in *Escherichia coli* and purified. GST pull-down was performed using these recombinant proteins and analyzed by western blot. **B.** Diffusional sizing of MBP-tagged PX-SNX5 or PX-SNX5-F136A with fluorescently labelled NCOA7-AS-NTD (NCOA7-AS-NTD-FITC) was measured using Fluidity One-M. Values represent means ± SD of 3 independent experiments. **C.** Recombinant MBP-tagged PX-SNX5, PX-SNX6 or MBP alone and GST-tagged NCOA7-AS-WT, NCOA7-AS-Y14A, NCOA7-AS-Y14F or GST alone were produced in *Escherichia coli* and purified. GST pull-down was performed using these recombinant proteins and analyzed by western blot.

Residue Tyr14 on NCOA7-AS is important for NCOA7-AS-mediated acidification of endolysosomes and antiviral activity against IAV

To assess the importance of NCOA7-AS-Y14 in the antiviral activity against IAV, we performed point mutations of NCOA7-AS-Y14 and stably expressed a negative control (Firefly), NCOA7-AS-WT, and NCOA7-AS-G91A, NCOA7-AS-Y14A or NCOA7-AS-Y14F mutants in A549 cells. Co-immunoprecipitation experiments first confirmed that NCOA7-AS-Y14A mutant did not interact with any of the 4 SNXs of interest. Minimal conservative NCOA7-AS-Y14F mutant conserved the interaction with SNX5 (and the other SNXs), confirming that the interaction between NCOA7-AS and SNX5 requires π-stacking between NCOA7-AS-Y14 and SNX5-F136 (Figure 5A).

While unable to interact with the V-ATPase (as illustrated with the lack of interaction with subunit ATP6V1E1, Figure 5A), NCOA7-AS-G91A still interacted with SNX5 and the other SNXs, suggesting that NCOA7-AS binding to the SNXs is not dependent on the binding to the V-ATPase.

Next, we tested the antiviral activity of these mutants against IAV in a single-cycle infection experiment. Compared to NCOA7-AS-WT, NCOA7-AS-Y14A was poorly functional with a significant reduction of antiviral activity against both A/Victoria/3/75 (Figure 5B) and A/WSN/1933 (Figure 5C). In contrast, NCOA7-AS-Y14F retained full antiviral activity despite being less expressed at steady state than NCOA7-AS-WT or the other mutants. The use of Lysotracker and Lysosensor showed that NCOA7-AS-Y14A had no impact on endolysosomal acidification, whereas NCOA7-AS-Y14F was as active as NCOA7-AS-WT (Figure 5D-E).

To further confirm these results, multicycle infection experiments were performed with A/WSN/1933 in A549 cells stably expressing a negative control (Firefly), NCOA7-AS-WT, NCOA7-AS-G91A, NCOA7-AS-Y14A or NCOA7-AS-Y14F (Figure 5F). Both NCOA7-AS-WT and NCOA7-AS-Y14F inhibited IAV infection by 2 logs at 24h and 48h, while NCOA7-AS-G91A and NCOA7-AS-Y14A had no impact on viral growth (similarly to the Firefly negative control). From 72h onwards, the antiviral effect of these proteins was not observed anymore.

Taken together, these data showed that residue Tyr14 on NCOA7-AS, which mediated the interaction with SNX5 and SNX6, was essential for antiviral activity against IAV and for inducing the endolysosomal overacidification.

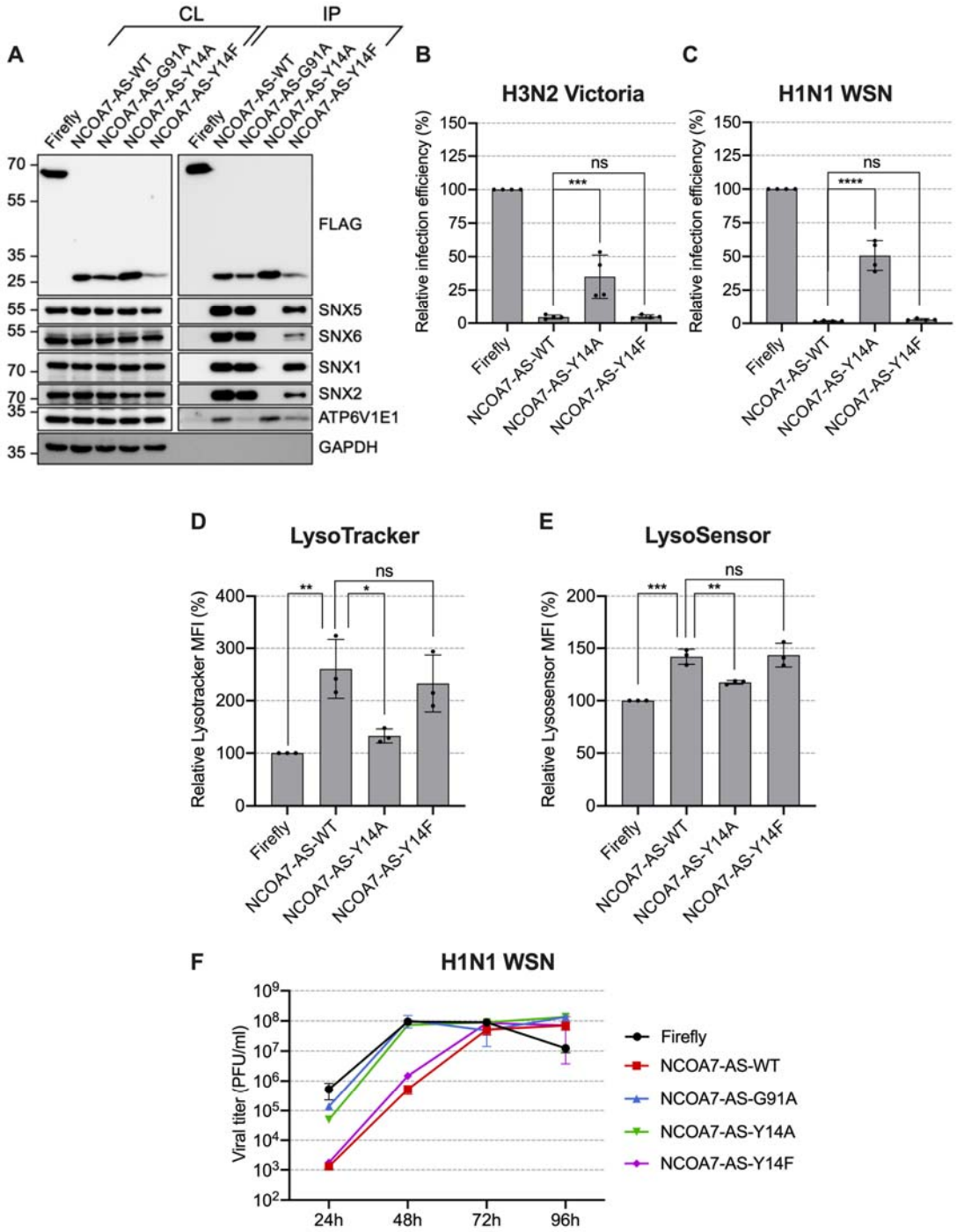

Figure 5. NCOA7-AS Tyrosine 14 is important for SNX5 binding, the inhibitory activity against IAV and the overacidification of the endolysosomal compartment. A. A549 cells stably expressing FLAG-tagged Firefly (Control), NCOA7-AS-WT, NCOA7-AS-G91A, NCOA7-AS-Y14A or NCOA7-AS-Y14F were lysed and the FLAG-tagged proteins were immunoprecipitated followed by immunoblotting analysis using anti-GAPDH (loading control), anti-FLAG, anti-SNX1, 2, 5 and 6 and anti-ATP6V1E1 antibodies. **B-C.** Cells stably expressing FLAG-tagged Firefly (Control), NCOA7-AS-WT, NCOA7-AS-Y14A or NCOA7-AS-Y14F were infected with Nanoluciferase-exrpressing A/Victoria/3/75 at an MOI of 0.5 (**B**) or A/WSN/1933 at an MOI of 0.25 (**C**). The relative infection efficiency was measured by monitoring Nanoluciferase activity at 8h post-infection. Data represent the mean and SD of four independent experiments.

D-E. Cells stably expressing FLAG-tagged Firefly (Control), NCOA7-AS-WT, NCOA7-AS-Y14A or NCOA7-Y14F were treated with 0.1 µM LysoTracker Green DND-26 (**D**) or with 0.1 µM LysoSensor Green DND-189 (**E**) for 1h at 37°C and the fluorescence intensity subsequently analyzed by flow cytometry. Data represent the mean and SD of three independent experiments. **F.** A549 cells stably expressing FLAG-tagged Firefly (Control), NCOA7-AS-WT, NCOA7-AS-G91A, NCOA7-AS-Y14A and NCOA7-AS-Y14F were infected with A/Victoria/3/75 at an MOI of 0.005 in multicycle replication conditions; the supernatants were harvested at the indicated time points post infection and infectious virus production was measured by plaque assays on MDCK cells. Data shows one representative experiment with the mean and SDs of technical triplicates.

Discussion

In this study, we characterized novel essential determinants for NCOA7-AS activity against IAV and its impact on the pH of the endolysosomal compartment. By defining NCOA7-AS' interactome, we identified SNX1, SNX2, SNX5 and SNX6 as novel binding partners of NCOA7-AS. These four SNXs seemed to play a role, at least to some extent, in NCOA7-AS-mediated overacidification of endosomes and lysosomes, with SNX1/2 having a significant impact. However, only SNX5 and SNX6 seemed to participate in NCOA7-AS antiviral activity against IAV, showing a potential decoupling between the acidification phenotype and the antiviral activity. Of note, double silencing of SNX1/2 or SNX5/6 affected the overall stability of the heterodimer, rendering the analysis of the contribution of these SNX in the anti-IAV activity of NCOA7-AS quite complex. These results, however, suggested that a sub-pool of SNX5/6, presumably not affected by the depletion of SNX1/2, could be important for NCOA7-AS antiviral activity. This phenotype is reminiscent of the restriction of *Chlamydia trachomatis* by SNX5/6, where depletion of SNX1/2 had no impact on bacterial replication, while depletion of SNX5/6 did, despite the recruitment of all four SNX-BARs (SNX1, SNX2, SNX5 and SNX6) to chlamydial inclusion membrane (Aeberhard et al., 2015; Mirrashidi et al., 2015). These results strengthen an emerging role of SNX5/6 independently of SNX1/2.

We were able to characterize in depth, biochemically and structurally, the interaction between SNX5/6 and NCOA7-AS. First, both full length NCOA7-AS and its N-terminal domain interacted directly with the PX domain of SNX5 and SNX6, as shown using recombinant proteins. Such a direct interaction was not observed with SNX1. We solved the X-ray structure of the PX-SNX5 domain bound to the N-terminal domain of NCOA7-AS, which enabled us to map the interface of interaction between the two partners. This showed a binding mode that was similar to the other cargoes of SNX5 (Sun et al., 2017; Simonetti et al., 2019). The N-terminal domain of NCOA7-AS interacted with the PX domain of SNX5 via the formation of a β-sheet with strands β1, β2, and β3 of SNX5 in a complementary groove at the base of the extended α-helical insertion (α2) of the PX SNX5 domain. This region corresponds to the 38 amino acid insertion in the PX domain that is uniquely present in SNX5 and SNX6, as well as their homologous protein SNX32, but not found in SNX1 and SNX2. This observation presumably explains why we could not detect a direct

interaction between NCOA7-AS and SNX1. Of note, the PX domain of SNX32 exhibits a high sequence homology with the PX domains of SNX5 and SNX6. However, SNX32 was not found in the interactome of NCOA7-AS, suggesting that it does not play a role in NCOA7-AS activity. This could be due to subtill differences in SNX32 sequence or subcellular localization as compared to SNX5 and 6, and would require further exploration.

The structure showed that the hydrophobic interaction mediated by SNX5 phenylalanine 136 and NCOA7-AS tyrosine 14, facing each other, seemed to be crucial. The essential role of these residues in the NCOA7-AS/SNX5 interaction was validated *in vitro*. The importance of NCOA7-AS tyrosine 14 was further confirmed in cells for the binding to SNX5, the overacidification phenotype induced by NCOA7-AS as well as its antiviral activity.

We also identified glycine 91 within the TLDc domain of NCOA7-AS as a critical residue mediating its interaction with the V1 subunits of the V-ATPase. This interaction is essential for both the overacidification of the endosomal compartment and the antiviral activity against IAV. Hence, our current model proposed that ectopic expression of NCOA7-AS disrupts the finely tuned pH gradient of the endolysosomal pathway through its interaction with the V-ATPase, thereby impairing IAV entry. V-ATPase activity is regulated through multiple mechanisms, including the dynamic assembly and disassembly of the V0/V1 complex (reviewed in (Maxson and Grinstein, 2014). Intriguingly, the Cryo-EM structure of the V-ATPase in complex with another TLDc protein, yeast OXR1, revealed that OXR1 inhibits V-ATPase activity by promoting complex disassembly (Khan et al., 2022). Consistently, the TLDc domains of human OXR1 and NCOA7-AS have also been shown to inhibit V-ATPase activity *in vitro* by inducing disassembly (Oot and Wilkens, 2024). These findings contrast with our own data. However, the *in vitro* study relied on purified, recombinant TLDc domains, which may not fully recapitulate the regulatory complexity present in a cellular context with the full-length proteins. Supporting this, a previous study showed that the long isoform of NCOA7 (NCOA7-FL) enhanced V-ATPase assembly and activity *in vivo* in mice (Castroflorio et al., 2021). Moreover, in human cells, NCOA7-AS ectopic expression clearly increases V-ATPase activity (Doyle et al., 2018) and this study). The apparent discrepancy between *in vitro* and *in vivo*/*ex vivo* data likely reflects the contribution of additional domains in NCOA7-AS and NCOA7-FL that influence the outcome of the TLDc–V-ATPase interaction. In support of this, we found that NCOA7-AS binding partners SNX1/2 (and to a lesser extent SNX5/6) are required for the overacidification of the endolysosomal compartment driven by NCOA7-AS. These findings underscore the importance of binding partners in modulating the activity of TLDc-containing proteins and add an additional layer of complexity to the regulation of V-ATPase function.

Together, these findings shed new light on the molecular mechanism of action of NCOA7-AS, defined novel essential cellular partners, as well as crucial residues for its antiviral activity.

Acknowlegdements

The authors acknowledge the Paul Scherrer Institute, Villigen, Switzerland for provision of synchrotron radiation beamtime at beamline PXIII-X06DA of the SLS. This work was funded by the National Research Agency (ANR-20-CE15-0010-02-CAIPIRINAS to CG, MB and MW), the European Research Council (ERC) under the European Union's Horizon 2020 research and innovation programme (grant agreement 759226, ANTIViR, to CG), the Institut National de la Santé et de la Recherche Médicale (INSERM) (to CG), a 3-year PhD studentship from the Ministry of Higher Education and Research (to AR), institutional funds from Centre National de la Recherche Scientifique (CNRS) and Montpellier University. OM and CG acknowledge support from the French research network on influenza viruses (ResaFlu; GDR2073) financed by the CNRS. Finally, the authors acknowledge the flow cytometry and imaging facility MRI, a member of the national infrastructure France-BioImaging supported by the French National Research Agency (ANR-10-INBS-04).

Disclosure and competing interest statement

The authors declare that they have no conflict of interest.

Author contributions

M.A.A, A.R., M.B. and C.G. designed the study, analyzed the data and wrote the manuscript. M.A.A. carried out the *in vitro* biochemical experiments, molecular cloning and western blots, obtained the crystals as well as analyzed the immunoprecipitation experiments. A.R. did molecular cloning and performed most of the virology and cellular experiments. M.T. provided technical assistance; together with CG, she prepared the mass spectrometry (MS) samples and did the silencing experiments, she did some molecular cloning and western blots. S.U. and K.E.K performed the MS analyses. E.R. and M.W. provided feedback and essential reagents. O.M. provided feedback and produced some IAV stocks. M.B. supervised the biochemical work and solved the crystal structures. All authors have read and approved the manuscript.

Materials and methods

Plasmids

The pRRL.sin.cPPT.SFFV/FLAG-E2-crimson-IRES-PuromycinR.WPRE, pRRL.sin.cPPT.SFFV/FLAG-Firefly-IRES-PuromycinR.WPRE and pRRL.sin.cPPT.SFFV/FLAG-NCOA7-AS-IRES-PuromycinR.WPRE have been

previously described (Doyle et al., 2018; Bonaventure et al., 2022). pRRL.sin.cPPT.SFFV/FLAG-NCOA7-AS-G91A-IRES-PuromycinR.WPRE, pRRL.sin.cPPT.SFFV/FLAG-NCOA7-AS-Y14A-IRES-PuromycinR.WPRE and pRRL.sin.cPPT.SFFV/FLAG-NCOA7-AS-Y14F-IRES-PuromycinR.WPRE were obtained by site-directed mutagenesis (overlap-extension PCR).

To express the C-terminal GST-tag version of NCOA7-AS recombinant proteins, a new pET30-MCS-cleavage site for Tobacco Etch Virus (TEV) protease-GST CDS-His6 CDS was created from the pET-30 Ek/LIC expression vector (Novagen). The NCOA7-AS full length, TLDc domain, N-terminal domain of NCOA7-AS, NCOA7-AS-Y14A and NCOA7-AS-Y14F CDS were PCR amplified from the aforementioned pRRL.sin.cPPT.SFFV/IRES-puro.WPRE lentiviral vector plasmid and cloned into the modified pET-30 expression vector using EcoRI and HindIII cloning sites.

Human SNX1, SNX5 and SNX6 cDNA were amplified by RT-PCR using the SuperScript III™ (Invitrogen) from mRNAs of A549 cells using the following primers: SNX1-forward 5'-TAAGCGGCCGCATGGCGTCGGGTGGTGGTGG -3'; SNX1-reverse 5'-AATTAATTAAGTCGACTTAGGAGATGGCCTTTGCCTCAGG-3'; SNX5-forward 5'-GGGCGGCCGCATGGCCGCGGTTCCCGAGTTGCTGC-3'; SNX5-reverse 5'-AATTAATTAAGTCGACTCAGTTATTCTTGAACAAGCTAAT-3'; SNX6-forward 5'-GTGGATCCATGATGGAAGGCCTGGACGACGGCCCGGAC-3'; SNX6-reverse 5'-ACCTCGAGTCATGTGTCTCCATTTAACACTGCC-3' and were cloned using NotI/SalI for SNX1 and SNX5, BamHI/XhoI for SNX6 in pRRL.sin.cPPT.SFFV/IRES-puro.WPRE.

The PX domain of SNX1, SNX5, and SNX6 were PCR-amplified from the aforementioned pRRL.sin.cPPT.SFFV/IRES-puro.WPRE lentiviral vector plasmids and cloned into pMAL-p4X expression vectors (New England Biolabs) (previously modified using BamHI and HindIII sites to add one KpnI restriction site), using KpnI and HindIII cloning sites. The pMAL-PX-SNX5-F136A was obtained by site-directed mutagenesis (overlap-extension PCR).

The PX-SNX5-beta strands NCOA7-AS CDS was PCR-amplified using an overlapping strategy to generate the chimeric protein and cloned into pET-30 Ek/LIC expression vectors (Novagen) using KpnI and SalI cloning sites. The insert is in frame with the S- and His-tags and a sequence encoding the Tobacco Etch Virus (TEV) protease cleavage site was inserted upstream of the chimera coding region to enable tag removal during the protein purification process. All plasmid constructs were verified by Sanger sequencing.

Cell lines, lentiviral vector production and transduction

Human cell line U87-MG (ARP-2188) were obtained from the AIDS reagent program. Madin-Darby canine kidney (MDCK), A549 cells, and HEK293T were gifts from Prof. W. Barclay (Imperial College London, UK) and Prof. M. Malim (King's College London, UK), respectively. These cell lines were maintained in Dulbecco's Modified Eagle Medium (DMEM) (Gibco) supplemented with 10% fetal bovine serum and 100 µg/mL penicillin and 100 units/ml streptomycin (Thermofisher). Lentiviral (LV) stocks were produced as described previously using polyethylenamine (Doyle

et al., 2018), either in HEK293T or in HEK293T LentiX (Clontech). Transduction with LVs was performed by incubating cells for 8 h prior to changing media for fresh media. Puromycin selection (2 µg/mL (Sigma-Aldrich)) was performed 24h post-transduction.

IAV production and infection

Nanoluciferase-coding A/WSN/33 (H1N1) and A/Victoria/3/75 (H3N2) (Diot et al., 2016; Doyle et al., 2018) were produced as previously described (Doyle et al., 2018). Briefly, the eight Pol I / PolII plasmids (0.5 µg each) for WSN rescue (a kind gift from Nadia Naffakh and Sandie Munier, Institut Pasteur Paris) or the eight Pol I plasmids (0.5 µg each) and four rescue plasmids (0.32 µg of PB1, PB2, PA and 0.64 µg NP plasmids) for Victoria virus rescue were co-transfected into HEK293T cells in 6-well plate format using Lipofectamine 3000 (Thermo Fisher Scientific). After 24h, the cells were detached and cocultured with MDCK cells in 25 mL flasks for 8h in DMEM containing 10% serum. The medium was then replaced with serum-free medium containing 1 µg/mL of L-1-p-Tosylamino-2-phenylethyl chloromethylketone (TPCK)-treated trypsin. Supernatants were used for virus amplification on MDCK cells. Viral stocks were titrated by plaque assays on MDCK cells.

For IAV single cycle infection, A549 cells stably expressing the constructs of interest were infected at an MOI of 0.5 for A/Victoria/3/75 (H3N2) and at an MOI of 0.25 for A/WSN/1933 for 1h in serum-free DMEM. The media was then replaced with DMEM containing 10% serum, and 8h post-infection, cells were washed with PBS and lysed in Passive Lysis Buffer (Promega). Levels of infection were measured using the Nano-Glo Luciferase Assay System (Promega).

Growth curve experiments

A549 stably expressing the constructs of interest were infected in triplicate in 12-well plates for 1h at an MOI of 0.005 with A/WSN/1933. Cells were then washed with PBS and incubated in 1mL of serum-free DMEM containing 1 µg/mL of TPCK-treated trypsin. Samples were collected at 24-, 48-, 72- and 96h post-infection and were titrated on MDCK cells by plaque assays.

siRNA transfection

Knock-downs were achieved by transfecting the indicated siRNAs (siCTRL1, siSNX1/2 and siSNX5/6) at a final concentration of 44 nM in A549 cells, with lipofectamine RNAimax (Thermo Fisher Scientific) according to the manufacturer's instructions for 72h. The scramble siRNA controls used were universal siCTRL1 (SIC001) (Sigma-Aldrich). The sequences of the siRNAs targeting the SNX had been described before (Simonetti et al., 2017): SNX1 (5′-AAGAACAAGACCAAGAGCCAC-3′), SNX2 (5′- AAGUCCAUCAUCUCCAGAACC-3′), SNX5 (5′-CUACGAAGCCCGACUUUGA-3′), and SNX6 (5′-UAAAUCAGCAGAUGGAGUA-3′) (Sigma-Aldrich).

Co-immunoprecipitation

U87-MG cells or A549 cells were transduced to stably express FLAG-NCOA7-AS, or mutants, FLAG-Firefly or FLAG-E2-Crimson. 25 million cells were lysed in lysis buffer (20 mM Hepes-NaOH pH 7.5; 150 mM NaCl; 1% NP-40 and protease inhibitor cocktail (Roche)). Lysates were clarified by centrifugation at 1,000 g for 10 min at 4°C. One fraction of cell lysates, corresponding to the whole-cell lysate was collected at this stage to serve as controls for protein input (10%) and the rest was incubated with FLAG-magnetic beads (Thermo Fisher Scientific) for 4h at 4°C. The beads were washed 5 times in lysis buffer and the immunoprecipitated proteins eluted using 150 µg/mL 3×FLAG peptide (Sigma-Aldrich) in lysis buffer for 2h at 4°C.

Mass spectrometry analysis

Sample digestion and peptides analysis were essentially performed as previously described (Sirvent et al., 2012). Briefly, purified proteins were loaded on an SDS-PAGE gel. After short migration, each sample was excised in one band. Proteins were digested using trypsin, and obtained peptides were analyzed online by nano-flow HPLC-nanoelectrospray ionization using a Qexactive HF mass spectrometer (Thermo Fisher Scientific) coupled to a nano- LC system (U3000-RSLC, Thermo Fisher Scientific). Desalting and preconcentration of samples were performed on-line on a Pepmap® precolumn (0.3 × 10 mm; Dionex). A gradient consisting of 0–40% B in A for 120 min (A: 0.1% formic acid, 2% acetonitrile in water, and B: 0.1% formic acid in 80% acetonitrile) at 300 nL/min, was used to elute peptides from the capillary reverse-phase column (0.075 × 500 mm, Pepmap®, Dionex). Data were acquired using Xcalibur software (version 4.1). A cycle of one full-scan mass spectrum (375–1,500 m/z) at a resolution of 60,000 (at 200 m/z), followed by 12 data-dependent MS/MS spectra (at a resolution of 30,000, isolation window 1.2 m/z) was repeated continuously throughout the nanoLC separation.

Raw data analysis was performed using the MaxQuant software (version 1.5.5.1) with standard settings. Used database consist of Human entries from Uniprot (reference proteome UniProt 2019_03) and 250 contaminants (MaxQuant contaminant database). Statistical analysis was performed using Perseus (v1.6.1.1). Intensity values were transformed in log2 scale and protein were filtered for at least three valid values in one of the experimental groups (NCOA7-AS or Control). Missing values were imputed by normal distribution (default parameter, assuming that most missing values are missing not at random and represent low abundance measurements). To highlight the proteins most abundant in NCOA7-AS vs Control, we used the built-in Two-sample test function in Perseus using standard parameters (Student's T-test, permutation base FDR, FDR of 5% and S0 of 0.1).

Immunoblot analysis

Cells were washed with PBS and were lysed in sample buffer (10 mM Tris–HCl pH7.6, 150 mM NaCl, 1% Triton X100, 1 mM EDTA, 0.1% deoxycholate, 2% SDS, 5% Glycerol, 100 mM DTT, 0.02% bromophenol blue). Cell lysates were resolved by SDS-PAGE and analyzed by immunoblotting using primary antibodies specific for

FLAG (M2, Sigma-Aldrich; 1/1,000), SNX1 (10304-1-AP, Proteintech; 1/1,000), SNX2 (611308, BD Biosciences; 1/1,000), SNX5 (17918-1-AP, Proteintech; 1/1,000), SNX6 (10114-1-AP, Proteintech; 1/1,000), ATP6V1A (17115-1-AP, Proteintech; 1/1,000), ATP6V1B2 (15097-1-AP, Proteintech; 1/1,000), ATP6V1E1 (15280-1-AP, Proteintech; 1/1,000), actin (A1978, Sigma-Aldrich; 1/5,000), followed by secondary horseradish peroxidase-conjugated anti-mouse or anti-rabbit immunoglobulin antibodies or primary GAPDH antibody coupled to horseradish peroxidase (HRP) GAPDH-HRP antibody (G9295, Sigma-Aldrich, 1/5,000) and primary FLAG antibody coupled to HRP FLAG-HRP antibody (G8592, Sigma-Aldrich, 1/10,000). Chemiluminescence was then measured using the Clarity ECL Western Blotting Substrate, Bio-Rad and a ChemiDoc™ gel imaging system (Bio-Rad).

Lysosomal compartment expansion and acidification

Transduced A549 cells were treated with 0.1 µM LysoSensor Green DND-189 or with 0.1 µM LysoTracker Green DND-26 for 1h at 37°C. Cells were then washed, trypsinized and analyzed immediately by flow cytometry on a BD LSRFortessa.

Protein expression and purification

GST tagged proteins

The recombinant plasmids pET-30 Ek/LIC expressing GST, NCOA7-AS-WT-GST and mutants, NCOA7-AS-TLDc-GST, NCOA7-AS-NTD-GST were transformed in an *Escherichia coli* BL21 (DE3) strain resistant to Phage T1 (New England Biolabs) carrying pRARE2. One colony was used to inoculate an overnight culture of 125 mL Lysogeny broth (LB) medium supplemented with kanamycin (50 µg/mL) and chloramphenicol (30 µg/mL). This culture was diluted in 2.5L of LB medium supplemented with the two antibiotics. The cells were grown at 37°C to an optical density at 600 nm of 0.8, then a 30 min cold shock on ice was performed and protein expression was induced with 1 mM Isopropyl-β-D-thiogalactoside (IPTG) and the culture was grown overnight at 16°C (except for GST for which bacteria were grown 3H at 37°C after adding IPTG). The cells were harvested by centrifugation at 8200g for 20 minutes and resuspended in 30 mL of buffer A (50 mM Tris–HCl pH 8, 400 mM NaCl, 5 mM β-mercaptoethanol, 40 mM imidazole, 10% glycerol and 1 mM benzamidine). The cells were disrupted by sonication and cell debris were removed by centrifugation at 28 000g for 60 minutes. The supernatant was loaded at 4°C on Ni–NTA agarose beads previously equilibrated with buffer A. The beads were washed once with buffer A and twice with buffer B (50 mM Tris–HCl pH 8, 1 M NaCl, 5 mM β-mercaptoethanol, 40 mM imidazole and 10% glycerol) and elution was performed with buffer E (50 mM Tris–HCl pH 8, 600 mM NaCl, 5 mM β-mercaptoethanol, 250 mM imidazole, 10% glycerol). The eluted protein was dialysed (dialysis-bag cutoff 12–15 kDa) against 1L dialysis buffer D (50 mM Tris–HCl pH 8, 600 mM NaCl, 5 mM β-mercaptoethanol, 10% glycerol) overnight at 4°C. After dialysis, the proteins were concentrated to 5 mg/mL using a Vivaspin® column (10 kDa cutoff, Sartorius), loaded onto a size-exclusion chromatography column (Superdex 200 increase 10/300 GL, GE Healthcare) and eluted with buffer F (50 mM

Tris–HCl pH 8, 600 mM NaCl, 5 mM β-mercaptoethanol, 10% glycerol). Aliquots of purified GST-tagged proteins were snap frozen in liquid nitrogen and stored at -80 °C.

MBP-tagged proteins

The recombinant plasmids pMAL-p4X expressing MBP-PX-SNX1, 5, and 6 were transformed in an *Escherichia coli* BL21 (DE3) strain resistant to Phage T1 (New England Biolabs) carrying pRARE2. One colony was used to inoculate an overnight culture of 125mL Lysogeny broth (LB) medium supplemented with kanamycin (50 µg/mL) and chloramphenicol (30 µg/mL). This culture was diluted in 2.5L of LB medium supplemented with the two antibiotics. The cells were grown at 37°C to an optical density at 600 nm of 0.8, then a 60 min cold shock on ice was performed, protein expression was induced with 1 mM Isopropyl-β-D-thiogalactoside (IPTG) and the culture was grown overnight at 16°C. The cells were harvested by centrifugation at 8 200g for 20 minutes and resuspended in 30 mL of buffer A (50 mM Tris–HCl pH 8, 400 mM NaCl, 5 mM β-mercaptoethanol, 10% glycerol and 1 mM benzamidine). The cells were disrupted by sonication and cell debris were removed by centrifugation at 28 000g for 60 minutes. The supernatant was loaded at 4°C on Amylose resin previously equilibrated with buffer A. The beads were washed once with buffer A and twice with buffer B (50 mM Tris–HCl pH 8, 1 M NaCl, 5 mM β-mercaptoethanol and 10% glycerol) and elution was performed with buffer E (50 mM Tris–HCl pH 8, 600 mM NaCl, 5 mM β-mercaptoethanol, 20 mM maltose, 10% glycerol). The eluted protein was dialysed (dialysis-bag cutoff 12–15 kDa) against 1L dialysis buffer D (50 mM Tris–HCl pH 8, 600 mM NaCl, 5 mM β-mercaptoethanol, 10% glycerol) overnight at 4°C. After dialysis, the proteins were concentrated to 5 mg/mL using a Vivaspin® column (10 kDa cutoff, Sartorius), loaded onto a size-exclusion chromatography column (Superdex 200 increase 10/300 GL, GE Healthcare) and eluted with buffer F (50 mM Tris–HCl pH 8, 600 mM NaCl, 5 mM β-mercaptoethanol, 10% glycerol). Aliquots of purified MBP-tagged proteins were snap frozen in liquid nitrogen and stored at -80°C.

GST pull-down

Recombinant GST-tagged proteins (14 to 35 µg) were incubated 2h at 4°C with glutathione agarose beads prewashed in pull-down assay buffer (50 mM Tris–HCl pH 8, 600 mM NaCl, 5 mM β-mercaptoethanol, 10% glycerol). Beads were then washed 3 times with pull-down assay buffer, then incubated for 2h at 4°C with 85 µg of recombinant MBP-tagged protein preincubated with glutathione agarose beads for 2h at 4°C. Beads were finally washed 3 times with pull-down assay buffer before adding 25 µl of Laemmli 2X. Samples were resolved by SDS-PAGE on a 10% acrylamide gel after 10 min boiling. Immunoblotting was performed by incubation with a primary GST antibody coupled to horseradish peroxidase (HRP) (A7340, Sigma-Aldrich) and a MBP antibody (E8032, NEB) followed by an HRP-conjugated secondary antibody. Bioluminescence was then measured (Clarity ECL Western Blotting Substrate, Bio-Rad) using a ChemiDoc system (Bio-Rad).

Kd determination

Recombinant MBP-PX-SNX5 and MBP-PX-SNX5-F136A were dialysed overnight at 4°C against 1L of PBS-10% glycerol. Concentrated proteins (0.38 µM to 250 µM) were mixed with 57 nM final FITC conjugated NCOA7-AS peptide (NH2-RLPLDIQIFY CARPDEEPFV KIITVEEAKR R-COOH) before loading on a Fluidity One chip. Hydrodynamic Radius were given by Fluidity One-W apparatus (Fluidic Analytics) and used to calculate Kd using the equation: $Y = Min + \frac{Max-Min}{1+(\frac{X}{IC50})^{Hill\ coefficient}}$.

Expression and purification of the chimera PX-SNX5-beta strands NCOA7-AS

The recombinant plasmid pET-30-PX-SNX5-beta strands NCOA7-AS was transformed in an *Escherichia coli* BL21 (DE3) strain resistant to Phage T1 (New England Biolabs) carrying pRARE2. One colony was used to inoculate an overnight culture of 125mL Lysogeny broth (LB) medium supplemented with kanamycin (50 µg/mL) and chloramphenicol (30 µg/mL). This culture was diluted in 2.5L of LB medium supplemented with the two antibiotics. The cells were grown at 37°C to an optical density at 600 nm of 0.8, then protein expression was induced with 1 mM Isopropyl-β-D-thiogalactoside (IPTG) and the culture was grown 3H at 37°C. The cells were harvested by centrifugation at 8 200g for 20 minutes and resuspended in 30 mL of buffer A (50 mM Tris–HCl pH 8, 400 mM NaCl, 5 mM β-mercaptoethanol, 40 mM imidazole, 10% glycerol and 1 mM benzamidine). The cells were disrupted by sonication and cell debris were removed by centrifugation at 28 000g for 60 minutes. The supernatant was loaded at 4°C on Ni–NTA agarose beads previously equilibrated with buffer A. The beads were washed once with buffer A and twice with buffer B (50 mM Tris–HCl pH 8, 1 M NaCl, 5 mM β-mercaptoethanol, 40 mM imidazole and 10% glycerol) and elution was performed with buffer E (50 mM Tris–HCl pH 8, 200 mM NaCl, 5 mM β-mercaptoethanol, 250 mM imidazole, 10% glycerol). The eluted protein was incubated with His-tagged Tobacco Etch Virus protease purified in our laboratory in a 1:100 (w:w) ratio; the cleavage reaction was performed during dialysis (dialysis-bag cutoff 12–15 kDa) against 1 L dialysis buffer D (50 mM Tris–HCl pH 8, 200 mM NaCl, 5 mM β-mercaptoethanol) overnight at 4 °C. After dialysis, the proteins were centrifuged for 20 min at 28 000g and the supernatant was loaded again at 4 °C on Ni–NTA agarose beads equilibrated with buffer D. The proteins without the His-tag were collected in the flow- through, concentrated to 5 mg/ml using a Vivaspin column (10 kDa cutoff, Sartorius), loaded onto a size-exclusion chromatography column (Superdex 75 Increase 10/300 Gl, GE Healthcare), and eluted with buffer F (50 mM Tris–HCl pH 8, 100 mM NaCl, 5 mM β-mercaptoethanol). Following this protocol, 3.5 mg pure protein was obtained from 1L culture.

Protein crystallization

Crystals of the trigonal form were obtained in sitting drops using the SwissCi (MRC) 96 well plate mixing 0.6 µL of protein solution concentrated to 17 mg/mL with 0.6 µL of reservoir solution made of 0.2 M Calcium acetate hydrate, 0.1M Sodium Cacodylate pH6.5 and 18% w/v polyethylene glycol 8000 and equilibrated against a reservoir volume of 50 µL at 18°C. The monoclinic crystals were obtained similarly by mixing 0.6 µL of protein solution concentrated to 17 mg/mL with 0.6 µL of reservoir solution made of 0.1M sodium citrate tribasic dihydrate pH 5.0, 30% v/v jeffamine® ED-2001 pH 7.0 and were not cryoprotected before being cryocooled.

X-ray Data collection and processing

Data collection was performed on the PXIII-X06DA beamline at the Swiss Light Source, Paul Scherrer Institute, Villigen, Switzerland. Data were processed and scaled with the XDS package (Kabsch, 2010). The phase problem was solved by molecular replacement using Phaser (McCoy, 2007) and the Phenix package (Liebschner et al., 2019), and the structure of the human SNX5 PX domain (5wy2) (Sun et al., 2017) as a search template. The structures were further manually rebuilt with Coot (Casañal et al., 2020) and refined with the Phenix package (Liebschner et al., 2019).

Statistical analyses

Statistical analyses were performed using GraphPad Prism software. Ordinary one-way ANOVA was used for all statistical analyses. p-values are indicated as the following: ns = not significant; $p < 0.05$ = *; $p < 0.01$ = **; $p < 0.001$ = ***; and $p < 0.0001$ = ****.

References

Aeberhard, L., Banhart, S., Fischer, M., Jehmlich, N., Rose, L., Koch, S., Laue, M., Renard, B.Y., Schmidt, F., Heuer, D., 2015. The Proteome of the Isolated Chlamydia trachomatis Containing Vacuole Reveals a Complex Trafficking Platform Enriched for Retromer Components. PLoS Pathog 11, e1004883. https://doi.org/10.1371/journal.ppat.1004883

Arnaud-Arnould, M., Tauziet, M., Moncorgé, O., Goujon, C., Blaise, M., 2021. Crystal structure of the TLDc domain of human NCOA7-AS. Acta Crystallogr F Struct Biol Commun 77, 230–237. https://doi.org/10.1107/s2053230x21006853

Blaise, M., Alsarraf, H.M.A.B., Wong, J.E.M.M., Midtgaard, S.R., Laroche, F., Schack, L., Spaink, H., Stougaard, J., Thirup, S., 2012. Crystal structure of the TLDc domain of oxidation resistance protein 2 from zebrafish. Proteins 80, 1694–1698. https://doi.org/10.1002/prot.24050

Bonaventure, B., Rebendenne, A., Valadão, A.L.C., Arnaud-Arnould, M., Gracias, S., Gracia, F.G. de, McKellar, J., Labaronne, E., Tauziet, M., Vivet-Boudou, V., Bernard, E., Briant, L., Gros, N., Djilli, W., Courgnaud, V., Parrinello, H., Rialle, S., Blaise, M., Lacroix, L., Lavigne, M., Paillart, J.-C., Ricci, E.P., Schulz, R.,

Jouvenet, N., Moncorgé, O., Goujon, C., 2022. The DEAD box RNA helicase DDX42 is an intrinsic inhibitor of positive-strand RNA viruses. EMBO Rep 23, e54061. https://doi.org/10.15252/embr.202154061

Burd, C., Cullen, P.J., 2014. Retromer: A Master Conductor of Endosome Sorting. Cold Spring Harbor Perspectives in Biology 6, a016774–a016774. https://doi.org/10.1101/cshperspect.a016774

Burda, P., Padilla, S.M., Sarkar, S., Emr, S.D., 2002. Retromer function in endosome-to-Golgi retrograde transport is regulated by the yeast Vps34 PtdIns 3-kinase. J Cell Sci 115, 3889–3900. https://doi.org/10.1242/jcs.00090

Carlton, J., Bujny, M., Peter, B.J., Oorschot, V.M.J., Rutherford, A., Mellor, H., Klumperman, J., McMahon, H.T., Cullen, P.J., 2004. Sorting nexin-1 mediates tubular endosome-to-TGN transport through coincidence sensing of high- curvature membranes and 3-phosphoinositides. Curr Biol 14, 1791–1800. https://doi.org/10.1016/j.cub.2004.09.077

Casañal, A., Lohkamp, B., Emsley, P., 2020. Current developments in *Coot* for macromolecular model building of Electron Cryo-microscopy and Crystallographic Data. Protein Science 29, 1055–1064. https://doi.org/10.1002/pro.3791

Castroflorio, E., Hoed, J. den, Svistunova, D., Finelli, M.J., Cebrian-Serrano, A., Corrochano, S., Bassett, A.R., Davies, B., Oliver, P.L., 2021. The Ncoa7 locus regulates V-ATPase formation and function, neurodevelopment and behaviour. Cell Mol Life Sci 78, 3503–3524. https://doi.org/10.1007/s00018-020-03721-6

Chandra, M., Chin, Y.K.-Y., Mas, C., Feathers, J.R., Paul, B., Datta, S., Chen, K.-E., Jia, X., Yang, Z., Norwood, S.J., Mohanty, B., Bugarcic, A., Teasdale, R.D., Henne, W.M., Mobli, M., Collins, B.M., 2019. Classification of the human phox homology (PX) domains based on their phosphoinositide binding specificities. Nat. Commun. 10, 1528. https://doi.org/10.1038/s41467-019-09355-y

Cheever, M.L., Sato, T.K., Beer, T. de, Kutateladze, T.G., Emr, S.D., Overduin, M., 2001. Phox domain interaction with PtdIns(3)P targets the Vam7 t-SNARE to vacuole membranes. Nat Cell Biol 3, 613–618. https://doi.org/10.1038/35083000

Cotter, K., Stransky, L., McGuire, C., Forgac, M., 2015. Recent Insights into the Structure, Regulation, and Function of the V-ATPases. Trends in Biochemical Sciences 40, 611–622. https://doi.org/10.1016/j.tibs.2015.08.005

Diot, C., Fournier, G., Santos, M.D., Magnus, J., Komarova, A., Werf, S.V.D., Munier, S., Naffakh, N., 2016. Influenza A Virus Polymerase Recruits the RNA Helicase DDX19 to Promote the Nuclear Export of Viral mRNAs. Sci Rep 6, 33763. https://doi.org/10.1038/srep33763

Dong, X., Yang, Y., Zou, Z., Zhao, Y., Ci, B., Zhong, L., Bhave, M., Wang, L., Kuo, Y.-C., Zang, X., Zhong, R., Aguilera, E.R., Richardson, R.B., Simonetti, B., Schoggins, J.W., Pfeiffer, J.K., Yu, L., Zhang, X., Xie, Y., Schmid, S.L., Xiao, G., Gleeson, P.A., Ktistakis, N.T., Cullen, P.J., Xavier, R.J., Levine, B., 2021. Sorting

nexin 5 mediates virus-induced autophagy and immunity. Nature 589, 456–461. https://doi.org/10.1038/s41586-020-03056-z

Dou, D., Revol, R., Östbye, H., Wang, H., Daniels, R., 2018. Influenza A Virus Cell Entry, Replication, Virion Assembly and Movement. Front. Immunol. 9, 1581. https://doi.org/10.3389/fimmu.2018.01581

Doyle, T., Moncorgé, O., Bonaventure, B., Pollpeter, D., Lussignol, M., Tauziet, M., Apolonia, L., Catanese, M.-T., Goujon, C., Malim, M.H., 2018. The interferon-inducible isoform of NCOA7 inhibits endosome-mediated viral entry. Nat Microbiol 3, 1369–1376. https://doi.org/10.1038/s41564-018-0273-9

Eaton, A.F., Brown, D., Merkulova, M., 2021. The evolutionary conserved TLDc domain defines a new class of (H+)V-ATPase interacting proteins. Sci Rep 11, 22654. https://doi.org/10.1038/s41598-021-01809-y

Elwell, C.A., Czudnochowski, N., Dollen, J.V., Johnson, J.R., Nakagawa, R., Mirrashidi, K., Krogan, N.J., Engel, J.N., Rosenberg, O.S., 2017. Chlamydia interfere with an interaction between the mannose-6-phosphate receptor and sorting nexins to counteract host restriction. eLife 6, e22709. https://doi.org/10.7554/elife.22709

Finelli, M.J., Oliver, P.L., 2017. TLDc proteins: new players in the oxidative stress response and neurological disease. Mamm Genome 28, 395–406. https://doi.org/10.1007/s00335-017-9706-7

Frost, A., Unger, V.M., Camilli, P.D., 2009. The BAR domain superfamily: membrane-molding macromolecules. Cell 137, 191–196. https://doi.org/10.1016/j.cell.2009.04.010

Gillooly, D.J., Raiborg, C., Stenmark, H., 2003. Phosphatidylinositol 3-phosphate is found in microdomains of early endosomes. Histochem Cell Biol 120, 445–453. https://doi.org/10.1007/s00418-003-0591-7

Helenius, A., 1992. Unpacking the incoming influenza virus. Cell 69, 577–578. https://doi.org/10.1016/0092-8674(92)90219-3

Kabsch, W., 2010. *XDS*. Acta Crystallogr D Biol Crystallogr 66, 125–132. https://doi.org/10.1107/s0907444909047337

Khan, H., Winstone, H., Jimenez-Guardeño, J.M., Graham, C., Doores, K.J., Goujon, C., Matthews, D.A., Davidson, A.D., Rihn, S.J., Palmarini, M., Neil, S.J.D., Malim, M.H., 2021. TMPRSS2 promotes SARS-CoV-2 evasion from NCOA7-mediated restriction. PLoS Pathog 17, e1009820. https://doi.org/10.1371/journal.ppat.1009820

Khan, Md.M., Lee, S., Couoh-Cardel, S., Oot, R.A., Kim, H., Wilkens, S., Roh, S., 2022. Oxidative stress protein Oxr1 promotes V-ATPase holoenzyme disassembly in catalytic activity-independent manner. The EMBO Journal 41, e109360. https://doi.org/10.15252/embj.2021109360

Kvainickas, A., Jimenez-Orgaz, A., Nägele, H., Hu, Z., Dengjel, J., Steinberg, F., 2017. Cargo-selective SNX-BAR proteins mediate retromer trimer independent retrograde transport. J Cell Biol 216, 3677–3693. https://doi.org/10.1083/jcb.201702137

Liebschner, D., Afonine, P.V., Baker, M.L., Bunkóczi, G., Chen, V.B., Croll, T.I., Hintze, B., Hung, L.-W., Jain, S., McCoy, A.J., Moriarty, N.W., Oeffner, R.D., Poon, B.K., Prisant, M.G., Read, R.J., Richardson, J.S., Richardson, D.C., Sammito, M.D., Sobolev, O.V., Stockwell, D.H., Terwilliger, T.C., Urzhumtsev, A.G., Videau, L.L., Williams, C.J., Adams, P.D., 2019. Macromolecular structure determination using X-rays, neutrons and electrons: recent developments in *Phenix*. Acta Crystallogr D Struct Biol 75, 861–877. https://doi.org/10.1107/s2059798319011471

Matlin, K.S., Reggio, H., Helenius, A., Simons, K., 1981. Infectious entry pathway of influenza virus in a canine kidney cell line. J Cell Biol 91, 601–613. https://doi.org/10.1083/jcb.91.3.601

Maxson, M.E., Grinstein, S., 2014. The vacuolar-type H+-ATPase at a glance - more than a proton pump. Journal of Cell Science 127, 4987–4993. https://doi.org/10.1242/jcs.158550

McCoy, A.J., 2007. Solving structures of protein complexes by molecular replacement with *Phaser*. Acta Crystallogr D Biol Crystallogr 63, 32–41. https://doi.org/10.1107/s0907444906045975

McKellar, J., Rebendenne, A., Wencker, M., Moncorgé, O., Goujon, C., 2021. Mammalian and Avian Host Cell Influenza A Restriction Factors. Viruses 13, 522. https://doi.org/10.3390/v13030522

Merkulova, M., Păunescu, T.G., Azroyan, A., Marshansky, V., Breton, S., Brown, D., 2015. Mapping the H+ (V)-ATPase interactome: identification of proteins involved in trafficking, folding, assembly and phosphorylation. Sci Rep 5, 14827. https://doi.org/10.1038/srep14827

Mirrashidi, K.M., Elwell, C.A., Verschueren, E., Johnson, J.R., Frando, A., Von Dollen, J., Rosenberg, O., Gulbahce, N., Jang, G., Johnson, T., Jäger, S., Gopalakrishnan, A.M., Sherry, J., Dunn, J.D., Olive, A., Penn, B., Shales, M., Cox, J.S., Starnbach, M.N., Derre, I., Valdivia, R., Krogan, N.J., Engel, J., 2015. Global Mapping of the Inc-Human Interactome Reveals that Retromer Restricts Chlamydia Infection. Cell Host & Microbe 18, 109–121. https://doi.org/10.1016/j.chom.2015.06.004

Oot, R.A., Wilkens, S., 2024. Human V-ATPase function is positively and negatively regulated by TLDc proteins. Structure 32, 989-1000.e6. https://doi.org/10.1016/j.str.2024.03.009

Paul, B., Kim, H.S., Kerr, M.C., Huston, W.M., Teasdale, R.D., Collins, B.M., 2017. Structural basis for the hijacking of endosomal sorting nexin proteins by Chlamydia trachomatis. eLife 6, e22311. https://doi.org/10.7554/elife.22311

Pinto, L.H., Holsinger, L.J., Lamb, R.A., 1992. Influenza virus M2 protein has ion channel activity. Cell 69, 517–528. https://doi.org/10.1016/0092-8674(92)90452-i

Pinto, L.H., Lamb, R.A., 2006. The M2 proton channels of influenza A and B viruses. J Biol Chem 281, 8997–9000. https://doi.org/10.1074/jbc.r500020200

Simonetti, B., Danson, C.M., Heesom, K.J., Cullen, P.J., 2017. Sequence-dependent cargo recognition by SNX-BARs mediates retromer-independent transport of CI-MPR. J Cell Biol 216, 3695–3712. https://doi.org/10.1083/jcb.201703015

Simonetti, B., Paul, B., Chaudhari, K., Weeratunga, S., Steinberg, F., Gorla, M., Heesom, K.J., Bashaw, G.J., Collins, B.M., Cullen, P.J., 2019. Molecular identification of a BAR domain-containing coat complex for endosomal recycling of transmembrane proteins. Nat Cell Biol 21, 1219–1233. https://doi.org/10.1038/s41556-019-0393-3

Sirvent, A., Vigy, O., Orsetti, B., Urbach, S., Roche, S., 2012. Analysis of SRC oncogenic signaling in colorectal cancer by stable isotope labeling with heavy amino acids in mouse xenografts. Mol Cell Proteomics 11, 1937–1950. https://doi.org/10.1074/mcp.m112.018168

Stauffer, S., Feng, Y., Nebioglu, F., Heilig, R., Picotti, P., Helenius, A., 2014. Stepwise priming by acidic pH and a high K+ concentration is required for efficient uncoating of influenza A virus cores after penetration. J Virol 88, 13029–13046. https://doi.org/10.1128/jvi.01430-14

Sun, Q., Yong, X., Sun, X., Yang, F., Dai, Z., Gong, Y., Zhou, L., Zhang, X., Niu, D., Dai, L., Liu, J.-J., Jia, D., 2017. Structural and functional insights into sorting nexin 5/6 interaction with bacterial effector IncE. Sig Transduct Target Ther 2, 17030. https://doi.org/10.1038/sigtrans.2017.30

Villalón-Letelier, F., Brooks, A.G., Saunders, P.M., Londrigan, S.L., Reading, P.C., 2017. Host Cell Restriction Factors that Limit Influenza A Infection. Viruses 9, 376. https://doi.org/10.3390/v9120376

Wang, R., Qin, Y., Xie, X.-S., Li, X., 2022. Molecular basis of mEAK7-mediated human V-ATPase regulation. Nat Commun 13, 3272. https://doi.org/10.1038/s41467-022-30899-z

Wassmer, T., Attar, N., Bujny, M.V., Oakley, J., Traer, C.J., Cullen, P.J., 2006. A loss-of-function screen reveals SNX5 and SNX6 as potential components of the mammalian retromer. Journal of Cell Science 120, 45–54. https://doi.org/10.1242/jcs.03302

Weering, J.R.T. van, Verkade, P., Cullen, P.J., 2010. SNX-BAR proteins in phosphoinositide-mediated, tubular-based endosomal sorting. Semin Cell Dev Biol 21, 371–380. https://doi.org/10.1016/j.semcdb.2009.11.009

Wharton, S.A., Belshe, R.B., Skehel, J.J., Hay, A.J., 1994. Role of virion M2 protein in influenza virus uncoating: specific reduction in the rate of membrane fusion between virus and liposomes by amantadine. J Gen Virol 75 (Pt 4), 945–948. https://doi.org/10.1099/0022-1317-75-4-945

Wickenhagen, A., Sugrue, E., Lytras, S., Kuchi, S., Noerenberg, M., Turnbull, M.L., Loney, C., Herder, V., Allan, J., Jarmson, I., Cameron-Ruiz, N., Varjak, M., Pinto, R.M., Lee, J.Y., Iselin, L., Palmalux, N., Stewart, D.G., Swingler, S., Greenwood, E.J.D., Crozier, T.W.M., Gu, Q., Davies, E.L., Clohisey, S., Wang, B., Costa, F.T.M., Santana, M.F., Ferreira, L.C.D.L., Murphy, L., Fawkes, A., Meynert, A., Grimes, G., Investigators, ISARIC4C, Filho, J.L.D.S., Marti, M., Hughes, J., Stanton, R.J., Wang, E.C.Y., Ho, A., Davis, I., Jarrett, R.F., Castello, A., Robertson, D.L., Semple, M.G., Openshaw, P.J.M., Palmarini, M., Lehner, P.J., Baillie, J.K., Rihn, S.J., Wilson, S.J., 2021. A prenylated dsRNA sensor protects against severe COVID-19. Science 374, eabj3624. https://doi.org/10.1126/science.abj3624

Yong, X., Zhao, L., Deng, W., Sun, H., Zhou, X., Mao, L., Hu, W., Shen, X., Sun, Q., Billadeau, D.D., Xue, Y., Jia, D., 2020. Mechanism of cargo recognition by retromer-linked SNX-BAR proteins. PLoS Biol 18, e3000631. https://doi.org/10.1371/journal.pbio.3000631

Yu, J.W., Lemmon, M.A., 2001. All Phox Homology (PX) Domains from Saccharomyces cerevisiae Specifically Recognize Phosphatidylinositol 3-Phosphate. Journal of Biological Chemistry 276, 44179–44184. https://doi.org/10.1074/jbc.m108811200

Zhirnov, O.P., 1990. Solubilization of matrix protein M1/M from virions occurs at different pH for orthomyxo- and paramyxoviruses. Virology 176, 274–279. https://doi.org/10.1016/0042-6822(90)90253-n

Supplementary Figures

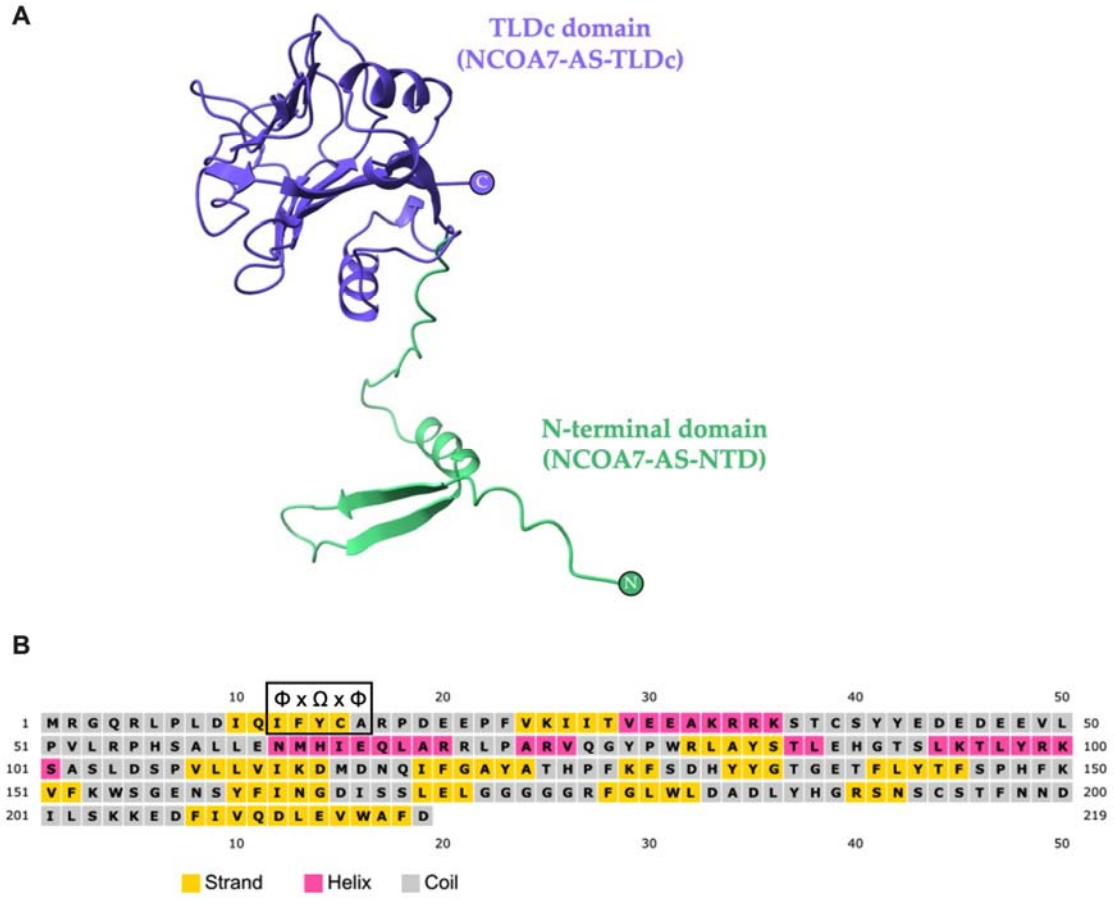

Supplementary Figure 1. A. AlphaFold prediction of NCOA7-AS with the N-terminal domain (NTD-amino-acids 1-53) colored in green and the C-terminal TLDc colored in purple. The NTD contains two antiparallel β-strands and a small α-helix. **B.** PSIPRED predictions, highlighting the presence of a ΦxΩxΦ (black box) in the first β-strand of NCOA7-AS.

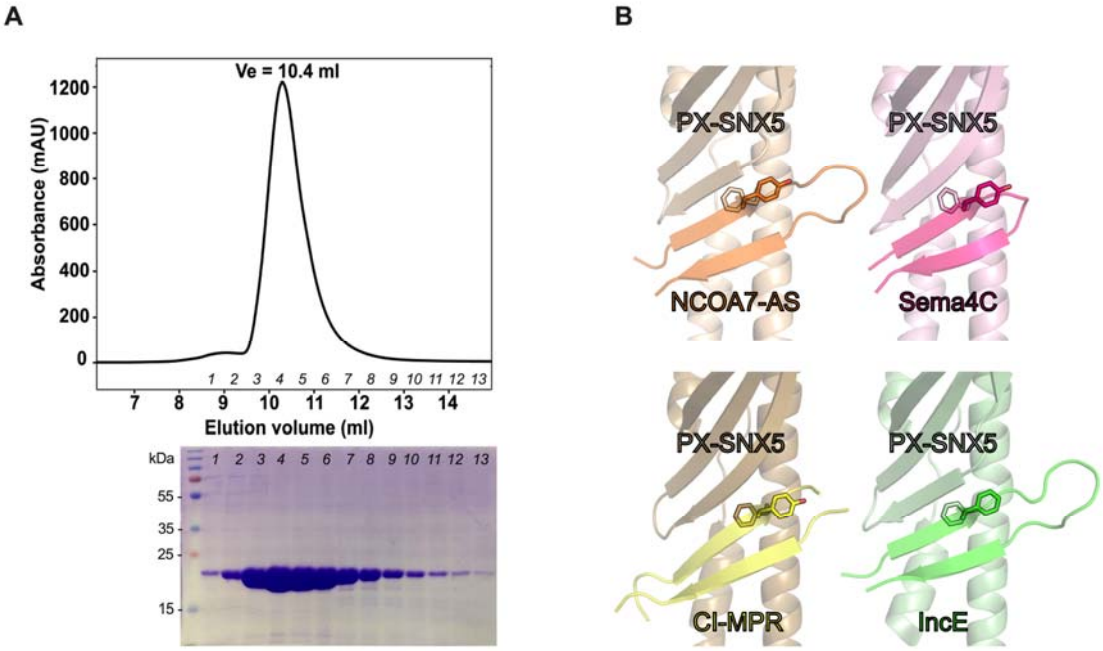

Supplementary Figure 2. A. The recombinant PX-SNX5-NCOA7-AS chimeric protein was produced in *Escherichia coli* and purified. The elution profile on Superdex 75 column is shown with the different fractions collected that have been analyzed by Coomassie staining. **B.** Comparison of the interface of PX-SNX5/NCOA7-AS with all the previously solved structure of PX-SNX5 bound to other binding partners. PX-SNX5::Sema4C (PDB: 6n5z), PX-SNX5::CI-MPR (PDB: 6n5y) and PX-SNX5::IncE (PDB: 5wy2).

Supplementary Tables

Supplementary Table 1. Mass Spectrometry data.
Detailed xlsx spreadsheet to download.

Summary Table:

Peptide counts (all)	Description	Symbol
55	Heat shock 70 kDa protein 4	HSPA4
50	**Sorting nexin-5**	**SNX5**
50	Heat shock cognate 71 kDa protein	HSPA8
47	**Sorting nexin-2**	**SNX2**
47;47	Heat shock 70 kDa protein 1A	HSPA1A
47;4	**Sorting nexin-6**	**SNX6**
46	**V-type proton ATPase catalytic subunit A**	**ATP6V1A**
46	Stress-70 protein, mitochondrial	HSPA9
45	**Sorting nexin-1**	**SNX1**
44	Heat shock protein 105 kDa	HSPH1
41;1	Protein transport protein Sec31A	SEC31A
36	ATP-dependent 6-phosphofructokinase, platelet type	PFKP
34	DNA replication licensing factor MCM6	MCM6
33;1	DNA replication licensing factor MCM4	MCM4
32;1	**V-type proton ATPase subunit C 1**	**ATP6V1C1**
31	**V-type proton ATPase subunit B, brain isoform**	**ATP6V1B2**
30	DNA replication licensing factor MCM7	MCM7
29	DNA replication licensing factor MCM2	MCM2
27;8	Tubulin beta chain	TUBB
27	Apoptosis-inducing factor 1, mitochondrial	AIFM1
25	**Nuclear receptor coactivator 7**	**NCOA7**
25	Splicing factor 3B subunit 3	SF3B3
21	Acetyl-coenzyme A synthetase, cytoplasmic	ACSS2
19	Poly(rC)-binding protein 1	PCBP1
15	**V-type proton ATPase subunit D**	**ATP6V1D**
15	Leucyl-cystinyl aminopeptidase	LNPEP
14;7	Heat shock 70 kDa protein 6	HSPA6
13;4	**V-type proton ATPase subunit E 1**	**ATP6V1E1**
12;10;9;7;1;1;1;1;1;1;1;1	POTE ankyrin domain family member E	POTEE
12;1	Synembryn-A	RIC8A
11	WD repeat-containing protein 7	WDR7
9	Bifunctional methylenetetrahydrofolate dehydrogenase/cyclohydrolase, mitochondrial	MTHFD2
9	Serine--tRNA ligase, mitochondrial	SARS2
9	Signal recognition particle receptor subunit beta	SRPRB
9	Protein SEC13 homolog	SEC13
7;2	**V-type proton ATPase subunit G 1**	**ATP6V1G1**
5	MOB kinase activator 1A	MOB1A
3	Replication factor C subunit 5	RFC5
2;1	Ras-related protein Rab-31	RAB31

Supplementary Table 2. X-ray data collection and refinement statistics

	Nt-NCOA7-PX-SNX5 Form I	**Nt-NCOA7-PX-SNX5 Form II**
PDB deposition code	9IAE	9IGY
Wavelength (Å)	1	1
Resolution range	48.1 - 2.3 (2.38 - 2.3)	46.1 - 2.3 (2.36 - 2.3)
Space group	$P\ 3_2\ 2\ 1$	$P\ 1\ 2_1\ 1$
Unit cell	63.13 63.13 101.51 90 90 120	46.9 76.99 110.85 90 100.181 90
Total reflections	210470 (25566)	230324 (29031)
Multiplicity	19.6 (20.14)	6.8 (7.0)
Completeness (%)	98.6 (100.00)	97.6 (99.9)
Mean I/sigma(I)	16.02 (2.23)	10.98 (1.61)
Wilson B-factor	37.3	38.6
R-meas (%)	19.3 (166.3)	16.2 (130.1)
CC1/2	0.999 (0.755)	0.997 (0.695)
Reflections used in refinement	10727 (1332)	33853 (2487)
Reflections used for R-free	1076 (106)	2015 (253)
R-work	0.201 (0.247)	0.227 (0.289)
R-free	0.239 (0.346)	0.262 (0.323)
Number of non-hydrogen atoms	1595	5665
macromolecules	1434	5437
solvent	161	228
Protein residues	173	665
RMSD (bonds, Å)	0.006	0.002
RMSD (angles, °)	0.52	0.41
Ramachandran favored	98.21	97.53

(%)		
Ramachandran allowed (%)	1.79	2.47
Ramachandran outliers (%)	0.00	0.00
Rotamer outliers (%)	1.25	0.81
Clashscore	3.16	3.24
Average B-factor (Å^2)	46.13	46.58
macromolecules	44.91	46.75
solvent	45.37	42.60

Statistics for the highest-resolution shell are shown in parentheses.